Effects of a sulfated exopolysaccharide produced by Altermonas infernus on bone biology.

Carmen Ruiz-Velasco, Marc Baud'Huin, Corinne Sinquin, Mike Maillasson,
Dominique Heymann, Sylvia Colliec-Jouault, Marc Padrines

Effects of a sulphated 'heparin-like' exopolysaccharide produced by *Altermonas infernus* on bone biology.

Authors: C. Ruiz Velasco[a,b], M. Baud'huin[a,b], C. Sinquin [c], M. Maillasson[d], D. Heymann[a,b,e], S. Colliec-Jouault[c], M. Padrines[a,b*].

[a] INSERM, U957, Nantes, F-44035, France

[b] Université de Nantes, Nantes Atlantique Universités, Laboratoire de Physiopathologie de la Résorption Osseuse et Thérapie des Tumeurs Osseuses Primitives, EA3822, Nantes, F-44035 France

[c] Laboratoire de Biotechnologie et Molécules Marines, Département Biotechnologies Marines, BIOMAR., IFREMER, Nantes F-44311, France

[d] INSERM U892 and IFR26- Ouest genopole, F-44035 France

[e] Centre Hospitalier Universitaire de Nantes, France

[*] **Corresponding author:**
Dr M. Padrines
EA 3822 - INSERM U957
Faculté de Médecine, 1 rue Gaston Veil
44035 Nantes cedex 01, France
Tel : 33 240 412 846 ; Fax : 33 240 412 860
E-mail : marc.padrines@univ-nantes.fr

Key words

Bone, exopolysaccharide, Glycosaminoglycan, Heparin

Abstract

The growth and differentiation of bone cells is controlled by various factors which can be modulated by heparan sulphates. Here, we investigated the effects of an oversulphated "heparin-like" exopolysaccharide (OS-EPS) on bone. We compared the effect of this compound with that of a native exopolysaccharide (EPS). Long-term administration of OS-EPS causes cancellous bone loss in mice due, in part, to an increase in the number of osteoclasts lining the trabecular bone surface. No significant difference in cancellous bone volume was found between EPS-treated mice and age-matched control mice, underlying the importance of sulphatation in trabecular bone loss. However, the mechanism sustaining this osteoporosis was unclear. To clarify OS-EPS activities, we investigated the effect of OS-EPS in osteogenesis. Our results demonstrated that OS-EPS inhibited osteoclastogenesis in two cell models. By surface plasmon resonance technique we revealed that OS-EPS can constitute a hetero-molecular complex OS-EPS/RANKL/RANK and that RANK had a higher affinity for RANKL pre-incubated with OS-EPS than for RANKL alone which would be in favour of an increase in bone resorption. However, *in vitro*, OS-EPS inhibit the early steps of osteoclast precursor adhesion and therefore inhibits the step of cell fusion. In addition, we showed that OS-EPS reduces the proliferation and accelerates osteoblastic differentiation, leading to strong inhibition of mineralized nodule formation, which would be in favour of an increase in bone resorption. Taken together, these data show different levels of bone resorption regulation by exopolysaccharides, most of them leading to proresorptive effects.

Introduction

Bone, a specialized connective tissue, is continually remodelled according to physiological events. This remodelling results from the activities of many cell lineages including mainly osteoblasts, osteocytes and osteoclasts. Their cellular interactions control their cellular activities and the bone remodelling intensity. These interactions can be established either through a cell–cell contact or by the release of many polypeptidic factors and/or their soluble receptor chains (cytokines, growth factors). These factors can act directly on osteogenic cells and their precursors to control differentiation, formation and functions (e.g. matrix formation, mineralization, resorption) (Kwan Tat *et al*., 2004). Among these factors, proteoglycans (PGs) appear critical for maintaining an appropriate number of osteoblasts and osteoclasts by modulating their proliferation and/or differentiation (Lamoureux *et al*., 2007).

PGs are composed of a core protein with covalently attached glycosaminoglycan (GAG) chains. These GAGs, linear polymers of repeated disaccharidic units, are sulphated and the number and position of sulphate are extremely variable in sulphated GAG depending on the tissular, cellular, and metabolic context, ensuring structural variability of these polysaccharides (Bernfield, 1999). These PGs are ubiquitous, being present as cell surface molecules anchored in the plasma membrane, as components of the insoluble extracellular matrix or as soluble molecules present in extracellular matrix and serum. PGs function in both cell–cell and cell–extracellular matrix adhesion and can also act to promote assembly of extracellular matrix molecules. Additionally, PGs bind a wide range of bioactive molecules, such as growth factors, chemokines, which regulate cell behaviour in normal and pathological processes. Thus, PGs or GAGs associated to the cell membrane or resident in the extracellular bone matrix regulated the bone growth and remodelling (Ruiz Velasco *et al*., 2010).

The osteoprotegerin (OPG)/Receptor Activator of NF-κB (RANK)/RANK Ligand (RANKL) molecular triad has been identified as members of a ligand-receptor system that directly regulates osteoclast differentiation and osteolysis (Simonet *et al*, 1997). While RANKL is a powerful inducer of bone resorption through its interaction with RANK (Kong *et al*., 1999), OPG acts as a decoy receptor for RANKL, thereby strongly inhibiting osteoclast differentiation (Yasuda *et al*., 1998). Any dysregulation of their respective expression leads to pathological conditions (Wittrant *et al*., 2004). OPG contains a heparin-binding domain and strongly bind to GAGs with a high affinity (K_D: 0.28 nM for heparin) (Theoleyre *et al*., 2006). Therefore, PGs decrease the bioavailability of OPG inducing its internalization (Standal *et al*., 2002, Kwan Tat *et al*., 2006) are involved in OPG-induced chemotaxis of monocytes (Mosheimer *et al*., 2005) and enhance the RANKL half-life at the cell membrane (Kwan Tat *et al*., 2006). Similarly to OPG, PGs interact with RANKL. For example, Shinmyouzu *et al*. (2007) showed that dermatan sulphate inhibits the binding of RANK to RANKL and reduce the RANKL-induced levels of MAPK signal transduction in osteoclast progenitors, thus abolishing osteoclastogenesis. These data demonstrate that PGs must be considered as essential co-factors modulating bone remodelling. Thus, PGs are not simply passive structural components of cells and extracellular matrices, rather, they are multifunctional molecules that regulate cell behaviour by fine tuning the function of many regulatory proteins (Lamoureux, 2009).

Heparin demonstrates several kinds of biological activities by binding to various extracellular molecules and plays pivotal roles in bone metabolism. However, the role of heparin in the biological activity of bone remains unclear. Recently, Ariyoshi *et al.* (2008) showed that heparin, after binding to RANKL, suppressed osteoclastogenesis and inhibited the formation of resorption pits induced by RANKL, whereas the other GAGs showed no effects. In contrast, Irie *et al.* (2007) showed that heparin specifically binds to OPG and

prevents OPG-mediated inhibition of osteoclastic bone resorption in the coculture of mouse bone marrow cells and osteoblasts and demonstrated that heparin enhances osteoclastic bone resorption by inhibiting OPG activity. Long-term heparin treatment causes cancellous bone loss in rats due in part to an increase in the number of osteoclasts lining the trabecular bone surface. However, results from various other groups suggest that GAGs, and in particular heparan sulphate (HS) and heparin, are potent co-stimulators of osteogenic signaling pathways (Zhao *et al*, 2006; Jackson *et al*, 2007; Ling *et al*, 2010)). Thus, the opportunity arises to leverage the stimulatory properties of HS-derived compounds as adjuvants for osteo-inductive therapies.

A broad series of polysaccharides has emerged as an important class of bioactive products (Franz and Alban, 1995; Bernas, 2003; Mayer and Lehmann, 2001). Polysaccharide-producing marine microorganisms occur widely in nature in different types of habitat (Sutherland, 1996), and some thermophilic and mesophilic polysaccharide-producing strains have been isolated from deep-sea hydrothermal vents (Guezennec, 2002; Nichols *et al*., 2005). *Alteromonas infernus,* classified as a non-pathogenic microorganism by the Institut Pasteur, secretes a water-soluble acidic heteropolysaccharide (Raguénès *et al*., 1997). The composition of this high-molecular-weight polysaccharide (10^6 g/mol) differs in monosaccharide content and/or ratio and sulphate content (10%) from other polysaccharides isolated from deep-sea hydrothermal bacteria and from polysaccharides of other origins. Structural characterization has shown that this exopolysaccharide is a highly branched acidic heteropolysaccharide composed of neutral sugars (glucose, galactose) and uronic acids (glucuronic acid and galacturonic acid) (Roger *et al*, 2004). The high-molecular-weight exopolysaccharide was chemically depolymerised and sulphated, with a view to obtaining a bioactive compound compatible with a therapeutic use (Roger *et al*, 2004). Highly sulphated low molecular-weight exopolysaccharide (40% sulphate groups, MW: 24 000, Fig. 1), with

uronic acid and sulphate contents comparable to those of heparin, were obtained without altering the osidic composition of this polymer (Guezennec *et al*., 1998). In contrast to the exopolysaccharide secreted by *Alteromonas infernus*, this oversulphated exopolysaccharide (OS-EPS) exhibits anticoagulant properties. It is less potent than low-molecular-weight heparin and unfractionated heparin (2.5 and 6.5 times, respectively), and should therefore carry a lower risk of bleeding (Colliec-Jouault *et al*., 2001). OS-EPS increases angiogenic properties of FGF-2 (Fibroblast growth factors-2) or VEGF (Vascular endothelial growth factor), i.e. endothelial cell proliferation and differentiation into vascular tubes; however it also inhibits the effect of FGF-2-induced cell migration (Matou *et al*., 2005). These angiogenic properties of OS-EPS are related to its sulphate content because no effect was observed with the native low molecular-weight exopolysaccharide (EPS). FGFs play an important major role in the control of cell proliferation, differentiation, and survival in several tissues including bone (Marie, 2003). Notably, FGF2 was found to promote cell growth and osteoblast differentiation in bone marrow-derived mesenchymal cells (Miraoui *et al*, 2009). In addition, FGF2 upregulate the expression of RANKL on rheumatoid arthritis synovial fibroblasts (Nakano *et al*., 2004). However, no data concerning the structure and biological activity of these exopolysaccharides on bone cells proliferation and differentiation were available until now. To explore its capacity to promote bone resorption or formation, an influence of OS-EPS on bone cell proliferation and differentiation was determined. OE-EPS was compared with EPS in order to study the effect of sulphate content on the biological properties of the exopolysaccharide.

Results

OS-EPS inhibits the proliferation of BMSCs during osteoblastic differentiation

To study the effect of OS-EPS on osteoblast precursors, we used the bone marrow stem cells (BMSCs) model, in which dexamethasone is known to induce osteoblast differentiation. Proliferation of BMSCs during osteoblastic differentiation was analyzed in the presence of OS-EPS. 25 µg/mL of OS-EPS significantly inhibited cell proliferation (Fig. 2A and 2B) in contrast to EPS. To determine whether these effects were due to inhibition of cell proliferation and/or induction of cell death, we used time-lapse microscopy to monitor the mitosis events. The results demonstrated a 70% inhibition of cell mitosis in the presence of 25µg/mL of OS-EPS after   48 h of culture as compared to the control (Fig. 2C). To determine whether the OS-EPS induced death in BMSCs by apoptosis, Hoechst staining and caspase-3 activation were investigated. Hoechst staining showed no modification of nuclear morphology in the presence of OS-EPS as compared to control cells (data not shown). Concerning the caspase-3 activity in BMSCs, the results showed that OS-EPS does not induce any activation of caspases (not shown). Flow cytometry of DNA content was performed to identify cell cycle perturbations following treatment with OS-EPS over a 48-h period in BMSCs. Although 24 h of OS-EPS treatment did not modulate the cell cycle in BMSCs (data not shown), 48 h of OS-EPS treatment induced a cell cycle arrest in G1 phases (Fig. 2D). Indeed, the number of cells in G1 phases increased from 73 ± 2 to 83 ± 3 % when treated with OS-EPS (Fig. 2D). This observation was concomitant with a reduction of cells in S and G2/M phases: 25 ± 3 versus 17 ± 2 % (Fig. 2D). EPS had no effect in any of the experimental conditions, underlying the importance of sulphatation in the proliferation.

OS-EPS inhibits mineralized nodule formation in pre-osteoblasts

To examine the role of OS-EPS on extracellular matrix mineralization in BMSCs cultures, BMSCs were treated for 17 days with OS-EPS, after which mineral was visualized by von Kossa staining. As demonstrated in Fig. 3A, OS-EPS dose-dependently inhibited mineralization with maximal inhibition occurring at 50 µg/mL. In late BMSCs culture, OS-EPS reduced the formation of bone nodules. To further understand the mechanism by which OS-EPS inhibits mineralization, cultures were treated with 25 µg/mL OS-EPS during days 3–17. OS-EPS reduced the formation of bone nodules when added in the two first weeks but not later (Fig. 3B), suggesting that OS-EPS blocks culture mineralization mainly by adversely affecting osteoblast differentiation and matrix deposition during the early matrix assembly stage and not by direct binding to hydroxyapatite crystals during the mineralization stage. Based on reduced mineralization, it was expected that OS-EPS would reduce expression of osteoblastic markers in cells. This study was performed on BMSCs under conditions where runt-related transcription factor 2 (Runx2), alkaline phosphatase (ALP) and type I collagen expression (Col1α1) were observed by preosteoblast stage, followed by bone sialoprotein (BSP) and osteocalcin (OC) by mature osteoblast stage. Unexpectedly, after 17 days of treatment, OS-EPS induced BSP and OC in a dose dependent manner (Fig. 3C). In contrast, OS-EPS reduced ALP, Runx2 and colα1 mRNA level in a dose dependent manner (Fig. 3C). However, Runx2 was transiently and strongly induced by OS-EPS; it increased after 7 days, reached a peak level at 10 days (14 days for the control), and decreased thereafter (Fig 3 C). This result clearly demonstrated an effect of OS-EPS on the osteoblastic differentiation. OS-EPS acted at the early steps of the process by affecting the preosteoblast and accelerating the osteoblactic differentiation.

OS-EPS inhibits RANKL-induced osteoclastogenesis in human models

CD14^{+} cells are human monocyte cells which can differentiate into tartrate-resistant acid phosphatase (TRAP)-positive multinucleated cells in 21 days upon RANKL stimulation. As shown in figure 4A, in contrast to EPS, addition of 0,5µg/ml OS-EPS, at the same time that RANKL addition, almost completely inhibited RANKL-induced osteoclastogenesis (p<0.01). We confirmed this effect in a second model of osteoclastogenesis. RAW 264.7 cells are murine monocyte/macrophage cells which can differentiate into TRAP-positive multinucleated cells in 5 days upon RANKL stimulation. OS-EPS completely inhibited RANKL-induced osteoclastogenesis of RAW 264.7 (results not shown). To better characterize the mechanisms by which OS-EPS inhibits osteoclast formation, the effect of OS-EPS were assessed at different times of the culture period. When OS-EPS was added 3 days before RANKL (D-3) to the culture, no osteoclasts were generated after 17 days (Fig. 4A) and the number of adherent CD14^{+} osteoclast precursors was decreased compared to the control condition. To determine whether these effects were due to induction of loss of adhesion, the effects of OS-EPS were evaluated by counting viable cells, as assessed by trypan blue exclusion. After the adherence of CD14^{+} cells in the wells, these cells were incubated with EPS or OS-EPS during 5 days. Blue trypan counting revealed that OS-EPS causes a loss of adherence of this type of cells (Fig. 4B). Thus in this culture condition, fewer osteoclast precursors adhered to the plastic surface and less osteoclasts were generated in the presence of RANKL. The addition of OS-EPS after one week culture step (D7) did not completely inhibit osteoclast formation (Figure 4A). OS-EPS acted at two distinct levels of osteoclastogenesis: i) at the early steps of the process by affecting and decreasing cell adherence and ii) at the end of the osteoclastogenesis process by inhibiting the spreading of the preformed osteoclasts. This result clearly demonstrated an effect of OS-EPS on RANKL-induced osteoclastogenesis. OS-EPS acted at the early steps of the process by affecting and decreasing cell adherence.

OS-EPS binds to RANKL

OPG/RANK and RANKL have been identified as members of a ligand-receptor system that directly regulates osteoclast differentiation and osteolysis. While RANKL is a powerful inducer of bone resorption through its interaction with RANK, OPG is a soluble decoy receptor and acts as a strong inhibitor of osteoclastic differentiation.

Surface plasmon resonance (SPR)-binding assays showed that recombinant full length OPG binds immobilized heparin (Theoleyre *et al.*, 2006). To determine the involvement of OS-EPS in the binding of OPG, we determined kinetic parameters by injecting different concentrations of OS-EPS over immobilized OPG and thus demonstrated a high-affinity OPG binding to OS-EPS (dissociation constant K_D: 0.22 nM) (Fig. 5). To explore the molecular mechanism underlying the effect of OS-EPS on RANKL-induced osteoclastogenesis, we investigated the molecular interactions between RANKL and OS-EPS by SPR. Surprisingly, OS-EPS was also able to bind to immobilized-RANKL, whereas EPS was not (Fig. 5A). We next compared OS-EPS activity to that of heparin, heparan sulphate, chondroitin sulphate and dermatan sulphate. None of the GAGs analyzed were able to bind to RANKL, with the exception of OS-EPS (Fig. 5A). Furthermore, using a single cycle kinetic assay, the K_D of OS-EPS for RANKL was 91 pM (Fig. 5).

Since RANKL is the natural ligand of RANK, we wondered whether OS-EPS could inhibit the complex RANKL–RANK present at the osteoclast membrane. We investigated the molecular interactions between OS-EPS, RANKL and RANK by SPR technique. We confirmed that RANK or RANKL bound to immobilized RANKL or immobilized RANK, respectively (Fig. 5B and 5C). While, in our conditions, OS-EPS did not bind to immobilized RANK (Fig. 5C), it bound to the preformed RANKL/RANK complex (Fig. 5B) thereby forming a ternary complex OS-EPS/RANKL/RANK. In addition, the pre-incubation of OS-

EPS (30 min at room temperature) with RANK or RANKL did not inhibit the capacity of OS-EPS to further bind to the preformed ternary complex OS-EPS/RANKL/RANK (data not shown). However, sensorgrams with RANKL, pre-incubated or not with OS-EPS, immobilized on the surface of a CM5 sensor chip revealed different binding response units for RANK (Fig. 5B). To determine the biophysical binding parameters for the ternary complex interactions, real-time SPR spectroscopy was performed (Fig. 6). Surprisingly, the kinetic study shows a significant increase of the association rate of RANK to RANKL pre-incubated with OS-EPS facilitating the complex formation. RANK had higher affinity for RANKL pre-incubated with OS-EPS surface sensor chips than for RANKL surface sensor chips (> 2-fold). This result would be in favour of an increase in bone resorption which has not been observed during the study of osteoclastogenesis (Fig. 4).

RANKL is not only a ligand for RANK but also acts as ligand for the decoy receptor OPG. To determine whether or not OS-EPS could affect the complex OPG/RANKL, RANKL has been immobilized on a sensor chip, and the capacity of OS-EPS to bind to complex OPG/RANKL was analyzed. Similar to the RANKL/RANK complex, OS-EPS is able to bind to a preformed OPG–RANKL complex (Fig. 5D and 5E) forming another ternary complex OS-EPS/RANKL/OPG. Also, the pre-incubation of OS-EPS (30 min at room temperature) with OPG or RANKL did not inhibit the capacity of OS-EPS to further bind to the preformed ternary complex OS-EPS/RANKL/OPG (data not shown). However, no modification of the kinetic parameters of the interaction of the OPG to RANKL pre-incubated with OS-EPS was observed.

OS-EPS induces trabecular bone loss.

During the 28 days of this study all of the mice from the different treatment groups (OS-EPS, EPS and heparin-treated) gained weight. No significant differences with respect to

weight gain were found between those mice treated with either OS-EPS or EPS or heparin or age-matched controls. However, at the femur level, micro-CT scanner analysis revealed that the mouse femur was characterized by large remodelling activities as compared to control femurs (Fig.7A). Thus, OS-EPS produced a reduction in cancellous bone volume when compared with control. The effect of OS-EPS on cancellous bone was similar to that of our positive control (heparin). OS-EPS did not modify the cortical bone volume (data not shown) but significantly reduced the trabecular bone volume ($p < 0.01$; Fig.7A). The trabecular number (Tb.N) was significantly reduced by OS-EPS ($p < 0.05$), whereas the trabecular space (Tb.Sp) increased ($p < 0.05$). Trabecular thickness (Tb.Th) was not significantly altered (Fig. 7). However, no significant difference in cancellous bone volume (BV/TV) was found between EPS-treated mice and age-matched control mice, underlying the importance of sulphatation in trabecular bone loss.

Histologic sections were stained with TRAP or ALP to quantify osteoclast or osteoblast surface-based data, respectively. Figure 7B shows that the parameter of osteoblast surface was not significantly different when comparing OS-EPS or EPS-treated mice and age-matched controls. In contrast, OS-EPS produced an increase in the percentage of cancellous bone covered by osteoclasts. Whereas mice given 6 mg/kg OS-EPS showed a 125% ± 23% ($p < 0.05$) increase in osteoclast surface, osteoclast surface was unaffected by treatment with EPS (Fig. 7B).

Discussion

In the present study, we have shown that long-term administration of OS-EPS, a `heparin-like' component (containing uronic acid and sulphate contents comparable to those of heparin) with `heparin-like' activity (anticoagulant properties), causes cancellous bone loss in mice due, in part, to an increase in the number of osteoclasts lining the trabecular bone surface. Our results are therefore similar to results published many years ago, in which long-term administration of heparin was shown to lead to the development of osteoporosis (Muir *et al.*, 1996). Similarly, Barbour *et al.* (1994) showed that 36% of pregnant women undergoing long-term heparin treatment had a 10% reduction in femoral bone mineral density. Both heparin (Muir *et al.*, 1996; Muir *et al.*, 1997, Rajgopal *et al.*, 2008) and OS-EPS increase the process of bone resorption. Although, heparin and OS-EPS has similar effects on osteoclast number, heparin was found to decrease osteoblast number (Muir *et al.*, 1996; Muir *et al.*, 1997, Rajgopal *et al.*, 2008), whereas OS-EPS has no effect. These effects resulting in bone loss begin early in the course of OS-EPS treatment (data not shown). However, the mechanism sustaining osteoporosis was unclear and it was difficult to determine if these effects on bone resorption were due to the direct effect of OS-EPS on osteoclasts or indirectly *via* its osteoblast activity.

GAGs exhibit several kinds of biological activities by binding to various extracellular molecules and play a pivotal roles in bone metabolism. An indirect proof of heparan sulphate proteoglycans (HSPGs) involvement in osteoclast functions was recently shown in a publication that demonstrated that heparanase, a HS-degrading endoglycosidase expressed in osteoblastic cells, stimulates bone formation and bone mass (Kram *et al.*, 2006). The effect of GAGs on osteoclastogenesis is controversial. For example, Ariyoshi *et al.* (2008) and Shinmyouzu *et al.* (2007) showed an inhibition of osteoclastogenesis after a direct interaction

14

of GAGs with RANKL. In contrast, Irie *et al.* (2007) showed a stimulation of osteoclastic bone resorption by inhibiting OPG activity. Our results clearly demonstrated that OS-EPS inhibited osteoclastogenesis in two systems tested. Furthermore, we demonstrated the importance of the sulphation of the exopolysaccharide in their inhibitory effect. Sulphation also plays a key role in GAGs biological activities as revealed by the present work. Sulphated polysaccharides enhance the biological activity of both homodimers and heterodimers of bone morphogenetic protein (BMP) by continuously serving the ligands to their signalling receptors expressed on cell membranes, similar to oversulphated chondroitine sulphate that binds to BMP-4 and enhances osteoblast differentiation (Miyazaki *et al*., 2008). Sulphation has clearly been shown to participate in to the control of cell biology. Kumarasuriyar *et al.* (2009) showed that the chlorate-induced-desulphation of GAGs expressed by MG63 cells delayed *in vitro* osteogenesis. In addition, sulphation strongly modulates the interaction of GAGs with proteins such as growth factors or enzymes (Lamoureux *et al.*, 2007; Gallagher, 2006).

However, the question remains of how we can explain the strong discrepancies between the *in vivo* and *in vitro* results. In this context, we first analyzed the interaction of OS-EPS with the OPG/RANK/RANKL molecular triad and the effect of OS-EPS on adhesion of osteoclast precursors. Here, we clearly showed that OS-EPS can constitute a hetero-molecular complex (OS-EPS /RANKL/RANK or OS-EPS/RANKL/OPG) as demonstrated by surface plasmon resonance technique and that RANK possesses a higher affinity for RANKL pre-incubated with OS-EPS than for RANKL alone. Contrarily, OS-EPS does not interfere in the binding of RANKL by OPG. These results also revealed that RANKL had higher affinity for OS-EPS (K_D = 91 pM) than for OPG (K_D = 0.27 nM, Kwan Tat *et al*, 2006). In conclusion, the preferential binding of RANKL to OS-EPS is able to facilitate the binary OS-EPS/RANKL complex formation, which, in turn, may facilitate the ternary OS-EPS/RANKL/RANK complex formation, which would be in favour of an increase of the bone

resorption. Secondly, we analyzed the effects of OS-EPS on adhesion of osteoclast precursors, demonstrating a sequential effect of OS-EPS on RANKL-induced osteoclastogenesis. OS-EPS inhibit the early step of osteoclast precursor adhesion and consequently inhibits the step of cell fusion. The alteration of cell adhesion and morphology prevents the cell fusion of osteoclast precursors and blocks osteoclast resorption which is particularly sensitive to cell morphology to develop their brush border (Rousselle and Heymann, 2002).

Our data are in favour of a direct inhibitory activity of OS-EPS on osteoclastogenesis and the effect observed *in vivo* may be explained by its effects on the bone osteoblast compartment and then by the dysregulation of the balance between osteoblasts and osteoclasts or by a slow-down of bone remodeling. The rate of bone formation is dependent on the commitment and replication of osteoprogenitor cells, their differentiation into functional osteoblasts and the life span of mature osteoblasts. Cells are committed to the osteoblast lineage by induction of the transcription factor Runx2 (Karsenty, 2001). This osteoblast differentiation is regulated by the actions of systemic and local signalling factors. Among these factors are FGFs, a family of polypeptides that control the proliferation and differentiation of osteoblast cell (Xiao *et al*., 2010). Thus, FGF2 is a powerful promoter of bone growth, enhancing mineralized nodule formation (Downey *et al*., 2009). This effect is mediated via HSPGs that coordinate the interaction of FGFs with their high-affinity tyrosine kinase receptors, the FGFRs (Eswarakumar *et al*., 2005). The interaction of PGs with FGFs provides a physiological mechanism for regulation of FGF signalling, FGFR1, and the extracellular signal-regulated kinase pathway. Furthermore, osteoclast differentiation and activity are regulated by GAGs at different levels, as revealed in previous studies. FGF-2 induces, after the binding to HS, the expression of RANKL and osteoclast maturation by rheumatoid synovial fibroblasts. FGF-2 not only augments the proliferation of rheumatoid synovial fibroblasts, but is also involved in osteoclast maturation, which leads to bone

16

destruction in rheumatoid arthritis (Nakano *et al.*, 2004 Matou *et al.* (2005) showed the binding of OS-EPS to FGF-2, therefore we hypothesize that FGF-2 can induce bone resorption after binding to OS-EPS.

Osteoblastic cells produce a complex extracellular matrix composed of a mixture of PGs, collagens and non-collagenous proteins. The interaction of PGs with matrix effector macromolecules via either their GAG chains or their protein core is critical in regulating a variety of cellular events. Alterations in the structural composition of the GAG/PG components of the extracellular matrix may have important consequences on cell proliferation and/or differentiation. Recently, Haupt *et al.* (2009) demonstrated the dependence of osteogenesis on specific HS chains, in particular those associated with glypican-3. The differentiating osteoblast-committed cells produce a homogenous HS species, which correlates with an increase in the HSPG glypican-3. Abrogation of glypican-3 reduces the expression of the osteogenic transcription factor Runx2. The data demonstrate tight linkage between HS modification and progression of osteogenic precursors through their developmental program.

Our results showed that (1) OS-EPS reduces expression of ALP, collαI, Runx2 (preosteoblast stage) in BMSCs cells and enhances OC and BSP mature osteoblast stage); (2) exogenous application of OS-EPS to cultures of primary BMSCs during *in vitro* differentiation completely blocks BMSC mineralization; (3) OS-EPS strongly reduces the proliferation of differentiating osteoblasts BMSCs cells. This proliferation inhibition was not due to an induction of apoptosis. These results suggest that OS-EPS reduces the proliferation and accelerates the osteoblastic differentiation, leading to strong inhibition of mineralized nodule formation that would be in favour of an increase of the bone resorption. However, these results cannot explain the effect observed *in vivo*. No significant difference in obsteoblast surface was found between OS-EPS-treated mice and age-matched control mice.

Although the explanation for these conflicting results is unclear, findings in a whole bone organ culture system are more likely to reflect events *in vivo* than those that occur in isolated osteoblast cultures. It is possible that this reflects the propensity of OS-EPS to bind to other critical growth factors, such as (1) bone morphogenetic protein (BMP). HS and chondroitine sulphate directly regulate the BMP-mediated differentiation of mesenchymal stem cells (hMSCs) into osteoblasts. BMPs, which have been shown to be heparin-binding proteins, induce osteoblast differentiation in hMSCs (Manton *et al.*, 2007). The role of heparin in the biological activity of BMP remains unclear. Heparin inhibits the binding of BMP-2 to BMPR and subsequent mRNA expression of Runx2, as well as phosphorylation of Smad and MAPK signal transduction. Furthermore, heparin was found to suppress the differentiation of osteoblastic MC3T3-E1 cells treated with BMP-2 (Kanzaki *et al*., 2008). In contrast, Zhao et al (2006) showed that heparin enhances BMP-induced osteoblast differentiation by protecting BMPs from degradation and inhibition by BMP antagonists; (2) tumor growth factorβ1 (TGFβ1), a known inhibitor of osteoprogenitor growth, which has a higher affinity than several other bone-related, heparin-binding growth factors (Manton *et al.*, 2006). This binding suggests that GAGs play a critical role in regulating TGF-β availability. Overcoming such sugar-mediated inhibition may prove important for wound repair. Given the importance of "heparin like" exopolysaccaharide for bone metabolism, it can be anticipated that OS-EPS due to its structural similarity with HS chains somehow interferes with the biological activities of these cell surface- and extracellular matrix-associated molecules. Taken together, these data show different levels of bone resorption regulation by GAGs or exopolysaccharides, most of them leading to proresorptive effects.

Materials and methods

Materials. Human M-CSF, human RANK and human OPG were obtained from R&D Systems (Abington, UK). Human RANKL was kindly provided by Amgen Inc. (Thousand Oaks, USA). Heparin sodium salt, heparan sulphate from bovine kidney, heparan sulphate from porcine intestinal mucosa, chondroitin sulphate from shark cartilage, dermatan sulphate from porcine intestinal mucosa and hyaluronic acid were purchased from Sigma (St Quentin Fallavier, France).

The two low molecular weight exopolysaccharides (EPS and OS-EPS) were obtained from high molecular weight exopolysaccharide by previously described procedures (Colliec-Jouault *et al*., 2001; Guezennec *et al*., 1998; Raguennes *et al.*, 1997). EPS and OS-EPS are homogenous fractions with an average molecular mass of 13 kDa and 24 kDa, and 10% and 40% sulphate groups, respectively, as determined by analytical high performance size-exclusion chromatography (Colliec-Jouault *et al*., 2001).

Culture medium and preparation of BMSCs. BMSCs were isolated from the bone marrow of 4 week-old Sprague-Dawley rats (Janvier, Le Genest Saint Isle, France). After anesthetization and cervical dislocation, femurs and tibias were dissected aseptically and cleaned of soft tissues. BMSCs were then flushed out with a syringe fitted with a 22-gauge needle containing maintenance media (MM) consisting of α-Minimal Essential Medium (α-MEM, Invitrogen) supplemented with 10% fetal calf serum (FCS) and 1% antibiotics (100 U/mL penicillin and 100 mg/L streptomycin). After centrifugation (5 minutes at 1600 rpm) cells were resuspended in 20 mL of MM. For osteogenic media (OM) culture conditions, this media was supplemented with 50 μg/mL ascorbic acid (Sigma) and 10^{-8} M dexamethasone (Sigma). Cells between passages 0 and 3 were used for all experiments. Cells were maintained at 37°C in a humidified atmosphere containing 5% CO_2.

Proliferation of BMSCs. Cells were plated (5×10^4/well) into a 6-well plate in MM overnight. Then MM was replaced by fresh OM in the presence or absence of 25 µg/mL EPS or OS-EPS, and cells were left to recover for 7 days (media was changed every 3 days). Then, cells in each well were washed three times in 1x Dulbecco phosphate-buffered saline (DPBS), trypsinized and counted in triplicate at day 3 and 7 by using blue trypan exclusion dye.

Induction of apoptosis. Programmed cell death was monitored microscopically following Hoechst staining. BMSCs were seeded at 10^4 cells/well in a 24-well plate and cultured for 24 h in MM. Then MM was replaced by fresh OM in the presence of 25 µg/mL OS-EPS for 24, 48, and 72 h or 100 nM staurosporine (Sigma) for 16 h as a positive control. At the end of the culture period, cells were stained with 10 µg/ml Hoechst reagent for 30 min at 37°C, and then observed under UV microscopy (DMRXA; Leica, Wetzlar, Germany).

Induction of apoptosis was also investigated by cleavage of caspase-3 substrates in supernatants of cultures with or without OS-EPS treatment. BMSCs were seeded at 15×10^3 cells/well (in a 24-well plate), then incubated with OS-EPS (25 µg/mL) for 24, 48, and 72 h. Cells incubated with 1 µM staurosporine for 6 h were used as positive controls. At the end of the incubation period, the cells were lysed with 50 µl of RIPA buffer for 30 min. The cells were then scraped off and protein content was quantified in parallel samples using the BCA (bicinchominique acid + Copper II sulphate) assay. Caspase-3 activity was assessed in 10 µl of the cell lysate with the kit CaspACEi Assay System (Fluorometric, Promega, Madison, USA) following the manufacturer's instructions.

Time-lapse microscopy. BMSCs were plated (2×10^3 cells/well) in triplicate into a 24-well plate in MM overnight. Then MM was replaced by fresh OM in the presence or absence of 25 µg/mL EPS or OS-EPS. Immediately post-treatment, the cultured dishes were placed onto a

time-lapse instrument (Leica) designed to capture transmission-phase images every 10 min from multiwell plates. Images were taken and edited using the MetamorphTM software. Cell divisions were then manually scored.

Cell cycle analysis. Cells were plated in triplicate (2×10^5/well) into a 6-well plate in MM overnight. Then MM was replaced by fresh OM in the presence or absence of 25 μg/mL EPS or OS-EPS. After 48 h cells were trypsinized and centrifuged at 1600 rpm for 3 min. Cell pellets were fixed in 70% ice-cold ethanol for 30 min and then washed twice in 100μl of DPBS. Cells were incubated in phosphate-citrate buffer at room temperature for 30 min then in DPBS containing 0.12% Triton X-100, 0.12 mM EDTA and 100 μg/ml ribonuclease A at 37ºC for 30 min. Cells were then centrifuged, washed twice and incubated in 50 μg/ml propidium iodide for 20 min at 4°C. Cell cycle distribution was analyzed by flow cytometry F500 (Beckman Coulter France) based on 2N and 4N DNA content using the MultiCycle software.

Mineralization Assay. BMSCs were plated (3.5×10^6 cells/well) in duplicate into a 24-multiwell plate in MM. After 24 hours of culture, the supernatant (MM) containing the non-adherent hematopoietic cells was removed. At confluence (72 h later), MM was replaced by OM (media was changed twice a week) in the presence of 25 μg/mL EPS or OS-EPS. After 1 week of culture, OM was supplemented with 10 mM β-glycerophosphate (Sigma) for 2 weeks (media was changed twice a week) in presence or absence of 25 μg/ml EPS or OS-EPS added at different times of the culture period. Then, Alizarin red staining (Alfa Aesar) was used to detect the mineralized nodules formed _in vitro_. Cells were washed in DPBS and fixed in 70% ice-cold ethanol for 1 h. The ethanol was then removed, and the fixed cells were washed three times with distilled water and incubated with alizarin red (40 mM, pH 7.4) for 10 minutes at

room temperature. After staining, excessive dye was washed gently with running water. Calcification deposits typically stained red. All experiments were performed three times.

Osteogenic differentiation Assay. BMSCs were plated (15×10^6 cells/well) into a 6-multiwell plate in MM. After 24 hours of culture, the supernatant (MM) containing the non-adherent hematopoietic cells was removed. At confluence (72 h later), MM was replaced by OM in the presence of 25 µg/mL EPS or OS-EPS (media was changed twice a week). After 1 week of culture, OM was supplemented with 10 mM β-glycerophosphate for 2 weeks (media was changed twice a week). For RT-qPCR analysis, total RNA was isolated from osteogenic culture at different times using the NucleoSpin II kit (Macherey-Nagel). RNA (500 ng) was reversed-transcribed (RT) using ThermoSript System (Invitrogen). cDNA synthesis was performed using total RNA with oligo(dT) at 50°C for 1 h. qPCR was performed in triplicate for each sample by using 5 µl 2x SYBR Green Supermix buffer (Bio-Rad, Marnes la Coquette, France), 1 µl cDNA, 300 nM of each primer, and DEPC H_2O to a final volume of 10 µl. After denaturing of cDNA at 98ºC for 30 sec, amplification and fluorescence determination were carried out in two steps: denaturation at 95ºC for 15 sec, and annealing and extension at 60ºC for 30 sec. The detection of SYBR Green was performed at the process of annealing. The sequence of the primers used in PCR reactions are shown in Table 1. Cyc1 cDNA as internal controls were used to normalize the data to determine the relative expression of the target genes. Polymerase chain reactions were carried out in 96-well plates using the Chromo4 System (Bio-Rad).

Gene	Gene (full name)	Accesion N°	Sequence	(5'→ 3')
ALP	Alkalin phosphatase	NM_013059.1	Forward: Reverse:	aggggcaactccatttttg ttgtaaccaggcccgttg
Runx2	runt-related transcription factor 2	NM_053470.1	Forward: Reverse:	cacagagctattaaagtgacagtgg aacaaactaggtttagagtcatcaagc
BSP	Bone Sialoprotein	NM_012587.2	Forward: Reverse:	cctactttttatcctcctctgaaacg tcgccatctccattttcttc
OC	Osteocalcin	NM_013414.1	Forward: Reverse:	aagcgcatctatggcaccac tcgagtcctggagagtagcc
Collα1	Alpha-1 type I collagen	NM_053304.1	Forward: Reverse:	catgttcagctttgtggacct gcagctgacttcagggatgt
Cyc1	cytochrome c-1	NM_001130491.1	Forward: Reverse:	tgctacacggaggaagaagc atcctcattagggccatcct

Differentiation of human CD14⁺ cells into osteoclasts. Human peripheral blood mononuclear cells (PBMCs) were isolated by centrifugation over Ficoll gradient (Sigma Chemicals Co., St. Louis, MO). CD14$^+$ cells were magnetically labeled with CD14 Microbeads and positively selected by MACS technology (Miltenyi Biotec, Bergisch Gladbach, Germany). CD14$^+$ cells were plated (45×10^3 cells/well) in triplicate into a 96-well plate in α-MEM containing 10% FCS and 25 ng/ml human M-CSF. After 3 days of culture, media was changed with fresh medium containing 10% FCS, 25 ng/ml human M-CSF, with or without 100 ng/ml hRANKL. Then medium was changed every 4 days. The formation of osteoclasts occurred around 14 days and was observed by tartrate-resistant acid phosphatase (TRAP) staining. In this experiment, EPS or OS-EPS were added at different times of the culture period. Then, multinucleated cells (>3 nuclei) were counted under a light microscope (Leica DM IRB, Nanterre, France; Camera: Olympus D70, Analysis software: Olympus DP Controller/Manager, Hamburg, Germany) after TRAP staining (Sigma, Saint Quentin-Fallavier, France)

Differentiation from the murine RAW 264.7 monocytic cell line. Murine RAW 264.7 monocytic cells (ATCC, Promochem, Molsheim, France) were cultured in phenol red-free α-Minimal Essential Medium (α-MEM) (Invitrogen, Eragny, France) supplemented with 10% fetal calf serum (FCS) (Perbio, Logan, USA) and 1% non essential amino acids (Invitrogen). To induce osteoclast formation, RAW 264.7 cells were scraped then incubated at 37°C for 2 minutes to allow adherence of the more differentiated cells. Non-adherent cells were then seeded in fresh medium at a density of $3x10^3$ cells/well in a 96-well plate. After 2 hours of culture, the medium was changed for fresh medium containing 100 ng/ml hRANKL with or without 0,5 µg/ml EPS or OS-EPS. The cells were stained histochemically for TRAP and the number of TRAP-positive multinuclear cells (MNCs) containing 3 or more nuclei was counted**.**

Adherence *of human CD14$^+$ cells.* Cells were plated ($25x10^4$ cells/well) in triplicate into a 96-well plate in α-MEM containing 10% FCS and 25 ng/ml human M-CSF during 3 days (time required for these cells to adhere). The medium was then replaced with fresh medium containing α-MEM, 10% FCS and 25 ng/ml human M-CSF in the presence of 1 µg/ml EPS or OS-EPS during 5 days (media were changed once). Then, non-adherent cells in the supernant were counted in triplicate by using blue trypan exclusion dye. The adherent cells were washed three times in DPBS, trypsinized and counted as above.

Surface plasmon resonance-binding assays. Experiments were carried out on a BIAcore 3000 instrument (BIAcore). RANKL, OPG (5 µg/ml in 10 mM acetate buffer, pH 4.0 and pH 5.0 (1:1;v/v)) and RANK (10 µg/ml in 10 mM acetate buffer, pH 5.0) were covalently immobilized to the dextran matrix of a CM5 sensor chip (BIAcore) via its primary amino groups at a flow rate of 30 µl/min. Immobilization levels ranging of 4000 resonance units

(RU) (RANKL and OPG) and 5000 RU (RANK) were obtained. EPS and OS-EPS K_D values for OPG, RANK and RANKL were determined using single cycle kinetics, starting with 1 nM OS-EPS or 100nM EPS (OPG), 250 nM OS-EPS or 2 µM EPS (RANKL) and 100 nM OS-EPS or 2 µM EPS (RANKL), then 1⁄2 dilutions. For binding analysis over the immobilized RANKL, OPG or RANK chip, the concentrations of 1 µg/ml OPG, 2 µg/ml RANK, 0.5 µg/ml RANKL, 20µM GAGs (heparin, or heparan sulphate, or chondroitin sulphate, or dermatan sulphate, or hyaluronic acid), 20 µM EPS and 200 nM OS-EPS were used. Binding assays were performed at 25ºC in 10 mM Hepes buffer, pH 7.4, containing 0.15 M NaCl and 0.005% P20 surfactant (HBS-P buffer, BIAcore) at a flow rate of 30 µl/min. Control sensorgrams (flow cell without RANKL, OPG and RANK) were automatically subtracted from the sensorgrams obtained with immobilized RANKL or OPG or RANK to yield true binding responses. The resulting sensorgrams were fitted using BiaEval 4.1 software (BIAcore).

Animal studies. twenty four 4-week-old male C3H/HeN male mice (Janvier, Le Genest Saint Isle, France) were housed under pathogen-free conditions at the Experimental Therapy Unit (Medicine Faculty of Nantes, France) in accordance with the institutional guidelines of the French Ethical Committee and under the supervision of authorized investigators. After 7 days of acclimatization these animals were assigned randomly to four groups: control (CT), heparin (Sigma H4784, 140U/mg, 50mg/ml), EPS and OS-EPS. All mice received (6 mg/kg) daily s.c. injection for a period of 28 days, consistent with the period of rapid growth in young mice. The 29th day, these animals were anesthetized with isoflurane (0.2% air, delivered via nosecone) and sacrificed by cervical dislocation. Bilateral femurs of each animal were dissected for histological studies and microarchitectural parameter quantification. Two independent experiments were performed.

Histological analysis. After sacrifice, left femur were cleaned from adjacent tissues and fixed in 10% buffered formaldehyde. Then samples were decalcified in 4% EDTA 0.2% paraformaldehyde (pH 7.4) buffer for 4 weeks and embedded in paraffin wax for TRAP and ALP staining. Five-µm-thick sections were cut through the femur (microtome: Leica SM 2500; Leica Instruments GmbH) and mounted on glass slides. Analysis and quantification of osteoblastic and osteoclastic areas were done using a Leica Q500 image analysis system.

Micro-computed tomography (µCT). After sacrifice, the right femur from each animal was dissected of soft tissues, fixed in 10% buffered formaldehyde and the distal metaphysis was used for micro-computed tomography (µ-CT) on a SkyScan-1072 (SkyScan, Aartselaar, Belgium). CT-Analyser software (from SkyScan) was used to analyse the structure of the sample, using the global segmentation method. Two-dimensional (2D) images were used to generate three-dimensional (3D) reconstructions and to calculate morphometric parameters with the SkyScan CtAn 3D creator software supplied with the instrument. Analysis was performed for the trabecular bone, whereby the trabecular region was precisely contoured in each single cross section manually. Bone volume ratio (BV/TV), trabecular thickness (Tb.Th), trabecular number (Tb.N) and trabecular space (Tb.Sp) were assessed.

Statistical analysis. All analyses were performed using GraphPad InStat v3.02 software (La Jolla, CA). The mean ± SD was calculated for all conditions and compared by ANOVA. In vivo experimentation results were analyzed with the unpaired nonparametric Mann–Whitney U test using two-tailed P-values. Differences relative to a probability of two-tailed $p < 0.05$ were considered significant.

Acknowledgments

Abbreviations

GAG : glycosaminoglycan

PG : proteoglycan

OPG : osteoprotegerin

RANK : Receptor Activator of NF-κB

RANKL : RANK Ligand

HS: Heparan Sulphate

EPS: ExoPolySaccharide

OS-EPS : oversulphated EPS

FGF: Fibroblast Growth Factor

VEGF: Vascular Endothelial Growth Factor

BMSC: Bone Marrow Stem Cell

ALP: Alkaline Phosphatase

Collα1: type 1 Collagen

BSP: Bone SialoProtein

OC: Ostéocalcin

SPR: Surface Plasmon Resonance

BMP: Bone Morphometric Protein

TGFβ: Tumor Growth Factor β

References

Ariyoshi W, Takahashi T, Kanno T, Ichimiya H, Shinmyouzu K, Takano H, Koseki T, Nishihara T. 2008. Heparin inhibits osteoclastic differentiation and function. *J. Cell. Biochem.* 103: 1707-1717.

Barbour LA, Kick SD, Steiner JF, LoVerde ME, Heddleston LN, Lear JL, Baron AE, Barton PL. 1994. A prospective study of heparin-induced osteoporosis in pregnancy using bone densitometry. *Am. J. Obstet. Gynecol.* 170 : 862-869.

Bernas GC. 2003. Angiotherapeutics from natural products: from bench to clinics? *Clin Hemorheol Microcirc.* 29: 199-203.

Bernfield M, Gotte M, Park PW, Reizes O, Fitzgerald ML, Lincecum J, Zako M. 1999. Functions of cell surface heparan sulphate proteoglycans. *Annu. Rev. Biochem.* 68:729-777.

Colliec-Jouault S, Chevolot L, Helley D, Ratiskol J, Bros A, Sinquin C, Roger O and Fischer AM. 2001. Characterization, chemical modifications and in vitro anticoagulant properties of an exopolysaccharide produced by Alteromonas infernus. *Biochim Biophys Acta.* 1528: 141–151.

Downey ME, Holliday LS, Aguirre JI, Wronski TJ. 2009. In vitro and in vivo evidence for stimulation of bone resorption by an EP4 receptor agonist and basic fibroblast growth factor: Implications for their efficacy as bone anabolic agents. *Bone.* 44: 266-274.

Eswarakumar VP, Lax I, Schlessinger J. 2005. Cellular signaling by fibroblast growth factor receptors. *Cytokine GrowthFactor Rev.* 16: 139–149.

Franz, G and Alban S. 1995. Structure-activity relationship of antithrombotic polysaccharide derivatives. *Int. J. Biol. Macromol.* 17: 311-314.

Gallagher JT. 2006. Multiprotein signalling complexes: regional assembly on heparin sulphate. *Biochem. Soc. Trans.* 34: 438-441.

Guezennec JG, Pignet P, Lijour Y, Gentric E, Ratiskol J, Colliec-Jouault S. 1998. Sulphation and depolymerization of a bacterial exopolysaccharide from hydrothermal origin. *Carbohydr Polymers.* 37: 19–24.

Guezennec J. 2002. Deep-sea hydrothermal vents: a new source of innovative bacterial exopolysaccharides of biotechnological interest? *J Ind Microbiol Biotechnol.* 29: 204–208.

Haupt LM, Murali S, Mun FK, Teplyuk N, Mei LF, Stein GS, van Wijnen AJ, Nurcombe V, Cool SM. 2009. The heparan sulphate proteoglycan (HSPG) glypican-3 mediates commitment of MC3T3-E1 cells toward osteogenesis. *J Cell Physiol.* 220: 780-791.

Irie A, Takami M, Kubo H, Sekino-Suzuki N, Kasahara, K, Sanai Y. 2007. Heparin enhances osteoclastic bone resorption by inhibiting osteoprotegerin activity. *Bone.* 41: 165- 174.

Jackson RA, Murali S, van Wijnen AJ, Stein GS, Nurcombe V, Cool SM. 2007. Heparan sulphate regulates the anabolic activity of MC3T3-E1 preosteoblast cells by induction of Runx2. *J Cell Physiol.* 210: 38-50.

Kanzaki S, Takahashi T, Kanno T, Ariyoshi W, Shinmyouzu K, Tujisawa T, Nishihara T. 2008. Heparin inhibits BMP-2 osteogenic bioactivity by binding to both BMP-2 and BMP receptor. *J Cell Physiol.* 216: 844-850.

Karsenty G. 2001. Minireview: transcriptional control of osteoblast differentiation. *Endocrinology.* 142: 2731-2733.

Kong YY, Yoshida H, Sarosi I, Tan HL, Timms E, Capparelli C, Morony S, Oliveira-dos-Santos AJ, Van G, Itie A, *et al.* 1999. OPGL is a key regulator of osteoclastogenesis, lymphocyte development and lymph-node organogenesis. *Nature.* 397: 315-323.

Kram V, Zcharia E, Yacoby-Zeevi O, Metzger S, Chajek-Shaul T, Gabet Y, Müller R, Vlodavsky I, Bab I. 2006. Heparanase is expressed in osteoblastic cells and stimulates bone formation and bone mass. *J Cell Physiol.* 207: 784-792.

Kumarasuriyar A, Lee I, Nurcombe V, Cool SM. 2009. De-sulphation of MG-63 cell glycosaminoglycans delays in vitro osteogenesis, up-regulates cholesterol synthesis and disrupts cell cycle and the actin cytoskeleton. *J Cell Physiol.* 219: 572-583.

Kwan Tat S, Padrines M, Theoleyre S, Heymann D, Fortun Y. 2004. IL-6, RANKL, TNF-alpha/IL-1: interrelations in bone resorption pathophysiology. *Cytokine Growth Factor Rev.* 15: 49–60.

Kwan Tat S, Padrines M, Théoleyre S, Couillaud-Battaglia S, Heymann D, Redini F, Fortun Y. 2006. OPG/membranous--RANKL complex is internalized via the clathrin pathway before a lysosomal and a proteasomal degradation. *Bone,* 39: 706-715.

Lamoureux F, Baud'huin M, Duplomb L, Heymann D, Redini F. 2007. Proteoglycans: key partners in bone cell biology. *Bioessays.* 29 : 758-771.

Lamoureux F, Picarda G, Garrigue-Antar L, Baud'huin M, Trichet V, Vidal A, Miot-Noirault E, Pitard B, Heymann D, Redini F. 2009. Glycosaminoglycans as potential regulators of osteoprotegerin therapeutic activity in osteosarcoma. *Cancer Res.* 69: 526-536.

Ling L, Dombrowski C, Foong KM, Haupt LM, Stein GS, Nurcombe V, van Wijnen AJ, Cool SM. 2010. Synergism between Wnt3a and heparin enhances osteogenesis via a phosphoinositide 3-kinase/Akt/RUNX2 pathway. *J Biol Chem.* [Epub ahead of print]

Manton KJ, Sadasivam M, Cool SM, Nurcombe V. 2006. Bone-specific heparan sulphates induce osteoblast growth arrest and downregulation of retinoblastoma protein. *J Cell Physiol.* 209: 219-229.

Manton KJ, Leong DF, Cool SM, Nurcombe V. 2007. Disruption of heparan and chondroitin sulphate signaling enhances mesenchymal stem cell-derived osteogenic differentiation via bone morphogenetic protein signaling pathways. *Stem Cells.* 25: 2845-2854.

Marie PJ. 2003. Fibroblast growth factor signaling controlling osteoblast differentiation. *Gene.* 316: 23-32.

Matou S, Colliec-Jouault S, Galy-Fauroux I, Ratiskol J, Sinquin C, Guezennec J, Fischer AM, Helley D. 2005. Effect of an oversulphated exopolysaccharide on angiogenesis induced by fibroblast growth factor-2 or vascular endothelial growth factor in vitro. *Biochem Pharmacol*. 69: 751-759.

Mayer AM, Lehmann VK. 2001. Marine pharmacology in 1999: antitumor and cytotoxic compounds. *Anticancer Res*. 21: 2489-2500.

Miraoui H, Oudina K, Petite H, Tanimoto Y, Moriyama K, Marie PJ. 2009. Fibroblast growth factor receptor 2 promotes osteogenic differentiation in mesenchymal cells via ERK1/2 and protein kinase C signaling. *J Biol Chem*. 284: 4897-4904.

Miyazaki T, Miyauchi S, Tawada A, Anada T, Matsuzaka S, Suzuki O. 2008. Oversulphated chondroitin sulphate-E binds to BMP-4 and enhances osteoblast differentiation. *J Cell Physiol*. 217: 769-777.

Mosheimer BA, Kaneider NC, Feistritzer C, Djanani AM, Sturn DH, Patsch JR, Wiedermann CJ. 2005. Syndecan-1 is involved in osteoprotegerin-induced chemotaxis in human peripheral blood monocytes. *J. Clin. Endocrinol. Metab*. 90 : 2964-2971.

Muir JM, Andrew M, Hirsh J, Weitz JI, Young E, Deschamps P, Shaughnessy SG. 1996. Histomorphometric analysis of the effects of standard heparin on trabecular bone in vivo. *Blood*. 88: 1314-1320.

Muir JM, Hirsh J, Weitz JI, Andrew M, Young E, Shaughnessy SG. 1997. A histomorphometric comparison of the effects of heparin and low-molecular-weight heparin on cancellous bone in rats. *Blood*. 89: 3236-3242.

Nakano, K., Okada, Y., Saito, K., Tanaka, Y., 2004. Induction of RANKL expression and osteoclast maturation by the binding of fibroblast growth factor 2 to heparan sulphate proteoglycan on rheumatoid synovial fibroblasts. *Arthritis Rheum*. 50: 2450-2458.

Nichols CA, Guezennec J, Bowman JP. 2005. Bacterial exopolysaccharides from extreme marine environments with special consideration of the southern ocean, sea ice, and deep-sea hydrothermal vents: a review. *Mar Biotechnol (NY)* 7: 253-271.

Raguénès G, Peres A, Ruimy R, Pignet P, R Christen R, Loaec M, Rougeaux H, Barbier G and Guezennec J. 1997. *Alteromonas infernus* sp.nov, a new polysaccharide producing bacterium isolated from a deep-sea hydrothermal vent. *J. Appl. Bacteriol*. 82: 422-430

Rajgopal, R., Bear, M., Butcher, M. K., Shaughnessy, S. G., 2008. The effects of heparin and low molecular weight heparins on bone. *Thromb. Res*. 12:, 293-298.

Roger O, Kervarec N, Ratiskol J, Colliec-Jouault S, Chevolot L. 2004. Structural studies of the main exopolysaccharide produced by the deep-sea bacterium Alteromonas infernus. *Carbohydr Res*. 229: 2371–2380.

Rousselle AV, Heymann D. 2002. Osteoclastic acidification pathways during bone resorption. *Bone*. 30: 533-540.

Ruiz Velasco C., Colliec-Jouault S., Redini F, Heymann D., Padrines M. 2010, Proteoglycans on bone tumor development. *Drug Discov. Today*. 15: 553-560.

Shinmyouzu K, Takahashi T, Ariyoshi W, Ichimiya H, Kanzaki S, Nishihara T. 2007. Dermatan sulphate inhibits osteoclast formation by binding to receptor activator of NF-kappa B
ligand. *Biochem. Biophys. Res. Commun*. 354: 447-452.

Simonet WS, Lacey DL, Dunstan CR, Kelley M, Chang MS, Luthy R, Nguyen HQ, Wooden S, Bennett L, Boone T *et al*. 1997. Osteoprotegerin: a novel secreted protein involved in the regulation of bone density. *Cell.* 89: 309-319.

Standal T, Seidel C, Hjertner O, Plesner T, Sanderson RD, Waage A, Borset M, Sundan A. 2002. Osteoprotegerin is bound, internalized, and degraded by multiple myeloma cells. *Blood.* 100: 3002-3007.

Sutherland IW. 1996. Biotechnology Second, completely revised edition, vol. 6, Products of primary metabolism, Rehm H. J. and Reed G. (eds), VCH, Weinheim, pp. 613-657.

Theoleyre S, Kwan Tat S, Vusio P, Blanchard F, Gallagher J, Ricard-Blum S, Fortun Y, Padrines M, Redini F, Heymann D. 2006. Characterization of osteoprotegerin binding to glycosaminoglycans by surface plasmon resonance: role in the interactions with receptor activator of nuclear factor kappaB ligand (RANKL) and RANK. *Biochem. Biophys. Res. Commun.* 34: 460-467.

Wittrant Y, Théoleyre S, Chipoy C, Padrines M, Blanchard F, Heymann D, Rédini F. 2004. RANKL/RANK/OPG: new therapeutic targets in bone tumours and associated osteolysis. *Biochim Biophys Acta.* 1704: 49-57.

Xiao L, Sobue T, Esliger A, Kronenberg MS, Coffin JD, Doetschman T, Hurley MM., 2010. Disruption of the Fgf2 gene activates the adipogenic and suppresses the osteogenic program in mesenchymal marrow stromal stem cells. *Bone*. 47: 360-370.

Yasuda H, Shima N, Nakagawa N, Mochizuki SI, Yano K, Fujise N, Sato Y, Goto M, Yamaguchi K, Kuriyama M, *et al*. 2004. Identity of osteoclastogenesis inhibitory factor (OCIF) and osteoprotegerin (OPG): a mechanism by which OPG/OCIF inhibits osteoclastogenesis in vitro. *Endocrinology.* 139: 1329-1337.

Zhao B, Katagiri T, Toyoda H, Takada T, Yanai T, Fukuda T, Chung UI, Koike T, Takaoka K, Kamijo R. 2006. Heparin potentiates the in vivo ectopic bone formation induced by bone morphogenetic protein-2. *J Biol Chem*. 281: 23246-23253.

Figure Legends

Figure 1: Branched nonasaccharidic repetitive unit of native EPS.

Figure 2: OS-EPS inhibits BMSCs proliferation during osteoblastic differentiation.
BMSCs were incubated in osteogenic media in the presence of 25µg/ml EPS or OS-EPS. After 7 days, images of treated cells were taken under light microscopy (**A**) and the number of viable cells was determined by trypan blue counting (*: p< 0.01) (**B**). Cumulative mitosis of the first 48h of incubation with of EPS or OS-EPS were manually scored from time-lapse analysis (**C**). Cell cycle distribution of BMSCs incubated with EPS or OS-EPS for 48 h was analyzed by propidium iodide staining and FACS analysis (**D**).

Figure 3: OS-EPS inhibits the extracellular matrix mineralization from BMSCs in a dose-dependent manner. (**A**) BMSCs were incubated in osteogenic media for three weeks in the presence or absence of increased concentrations of EPS and OS-EPS. (**B**) EPS or OS-EPS at 25µg/ml were added at different times of the culture period as indicated. At the end of the culture period, Alizarin Red staining was performed (original magnification x 10). (**C**) Gene expression profiles of bone-specific markers of osteoblastic differentiation were determined by qPCR in absence (CT) or in presence of different OS-EPS concentration, The data represent fold difference in expression following normalization against Cyc1.

Figure 4: OS-EPS inhibits RANKL-induced osteoclatogenesis and cell adhesion of human CD14^{+} monocytes. (**A**) CD14^{+} purified monocytes were first cultured for 3 days in 25 ng/ml hM-CSF to achieve a complete cell adhesion. For osteoclastogenesis experiments, cells were then incubated for 15 days in the presence of 25 ng/ml hM-CSF with or without hRANKL (100 ng/ml). EPS or OS-EPS (0,5µg/ml) were added at different time points during

the culture period, as indicated: -3 days indicates the culture condition with only 25 ng/ml of hM-CSF (cellular adhesion period); 0→14 days indicate the period with 25 ng/ml of hM-CSF and 100 ng/ml of RANKL (Osteoclastic differentiation period). At the end of the culture period, TRAP staining was performed (original magnification x 40) and TRAP positives multinucleated cells (more than 3 nuclei) were counted under a light microscope. (**B**) For adherence experiments, cells were incubated for 5 days in the presence of EPS or OS-EPS at 1µg/ml. The non-adherent cells in the supernant were counted in triplicate by using blue trypan exclusion dye. The adherent cells were washed three times in 1x Dulbecco phosphate-buffered saline (DPBS), trypsinised and counted as above.
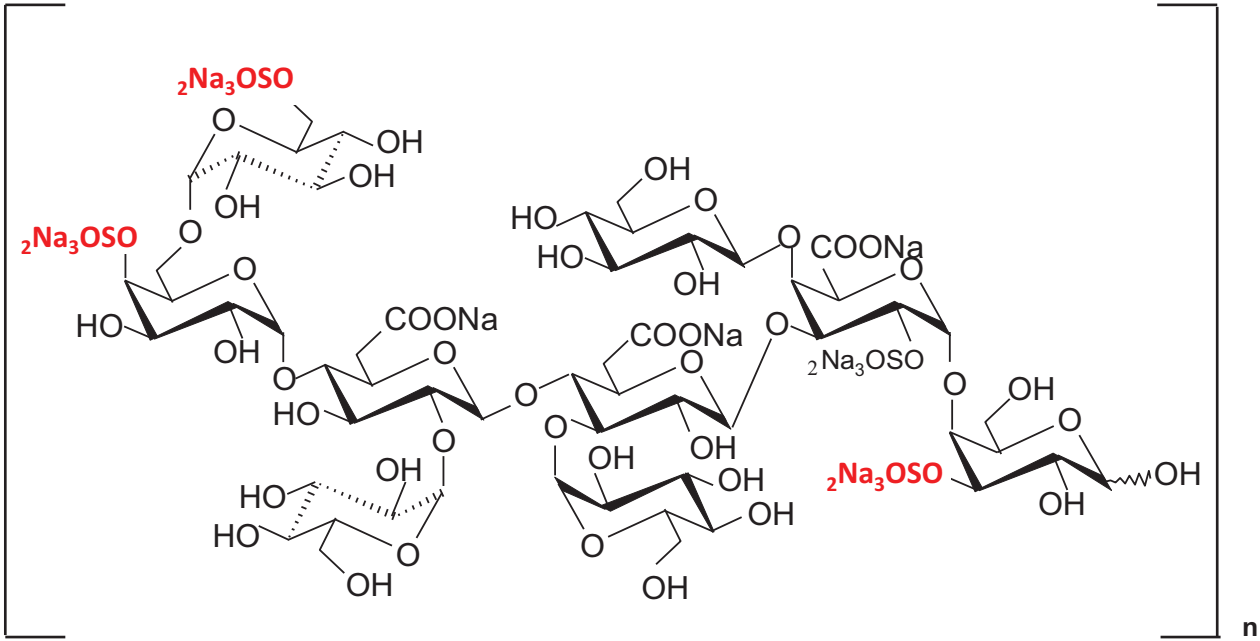
Figure 5: OS-EPS binds RANKL. Experiments were carried out on a BIAcore 3000 instrument (BIAcore). GAGs (20µM), or EPS (20 µM), or OS-EPS (2µM) were injected at a flow rate of 30 µl/min over the immobilized-RANKL sensorchip (**A**). RANK (2µg/ml), or RANKL (0.5µg/ml) or OS-EPS (200nM) or OPG (1µg/ml) were injected at a flow rate of 30 µl/min over the immobilized-RANKL sensorchip (**B, D**) or over the immobilized-RANK (**C**) or over the immobilized-OPG (**E**). EPS and OS-EPS K_D values for immobilized OPG, RANK and RANKL were assessed (**Table**).

Figure 6: OS-EPS facilitates the binding of RANK-RANKL. Real-time SPR binding analyses of interactions of RANK and RANKL pre-incubated or not with OS-EPS. Sensorgrams were recorded with RANKL (**A**) or RANKL pre-incubated with OS-EPS (**B**) immobilized on CM5 sensor chips, and injections of RANK solutions [50, 25, 12.5, 6.25, and 3.125 nM RANK], using a BIAcore 3000 biosensor and BiaEval 4.1 software. The kinetic and thermodynamic values were ka $(M^{-1}s^{-1})$ = 5.28 10^5; kd (s^{-1}) = 1.27 10^{-3} and K_D = 2.39 nM for

RANKL in (**A**), and ka $(M^{-1}s^{-1}) = 1.23 \ 10^6$; kd $(s^{-1}) = 1.32 \ 10^{-3}$ and $K_D = 1.09$ nM for RANKL pre-incubated with OS-EPS in (**B**).

Figure 7: OS-EPS reduces trabecular bone. Twenty four 4-week-old male C3H/HeN male mice received daily s.c. injection of DPBS, EPS, OS-EPS or heparin (6 mg/kg) for a period of 28 days. (**A**) Right femur of each animal was dissected for microarchitectural parameter quantification. The distal metaphysis were used for micro-computed tomography (μ-CT) on a SkyScan-1072 (SkyScan, Aartselaar, Belgium). μCT-Analyser software SkyScan was used to analyse the structure of the samples. Bone volume ratio (BV/TV), trabecular thickness (Tb.Th), trabecular number (Tb.N) and trabecular separation (Tb.Sp) were assessed (**Table**). (n= 6 by groups). (*: $p < 0.05$). (**B**) Analysis and quantification of osteoblastic and osteoclastic areas were done using a Leica Q500 image analysis system after TRAP and ALP staining, respectively. Two independent experiments were performed (n= 6 by groups). (*: $p < 0.05$).

Figure 1

SO$_3$Na$_2$: native EPS
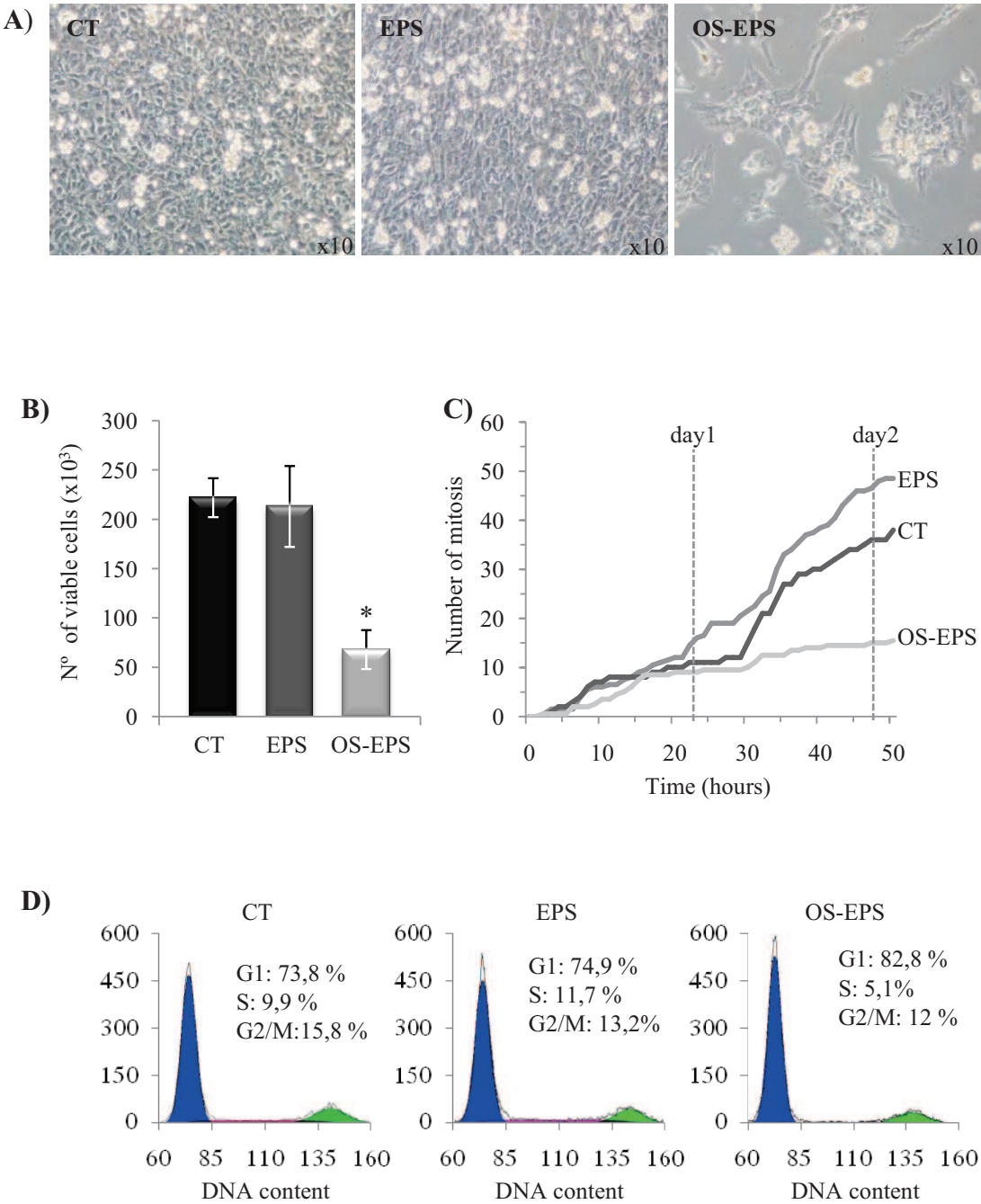**SO$_3$Na$_2$** : OS-EPS after O-Sulfatation

Figure 2

A)

B)

C)

D)

Figure 3

A)

B)

C)

Figure 4

Figure 5

A)

	K_D (pM)	
	EPS	OS-EPS
RANKL	>µM	91
OPG	15400	220
RANK	No binding	>µM

Dissociation constant (K_D) of EPS and OS-EPS with human RANK and OPG and RANKL obtained by SPR

B)

C)

D)

E)

Figure 6

Figure 7

A)

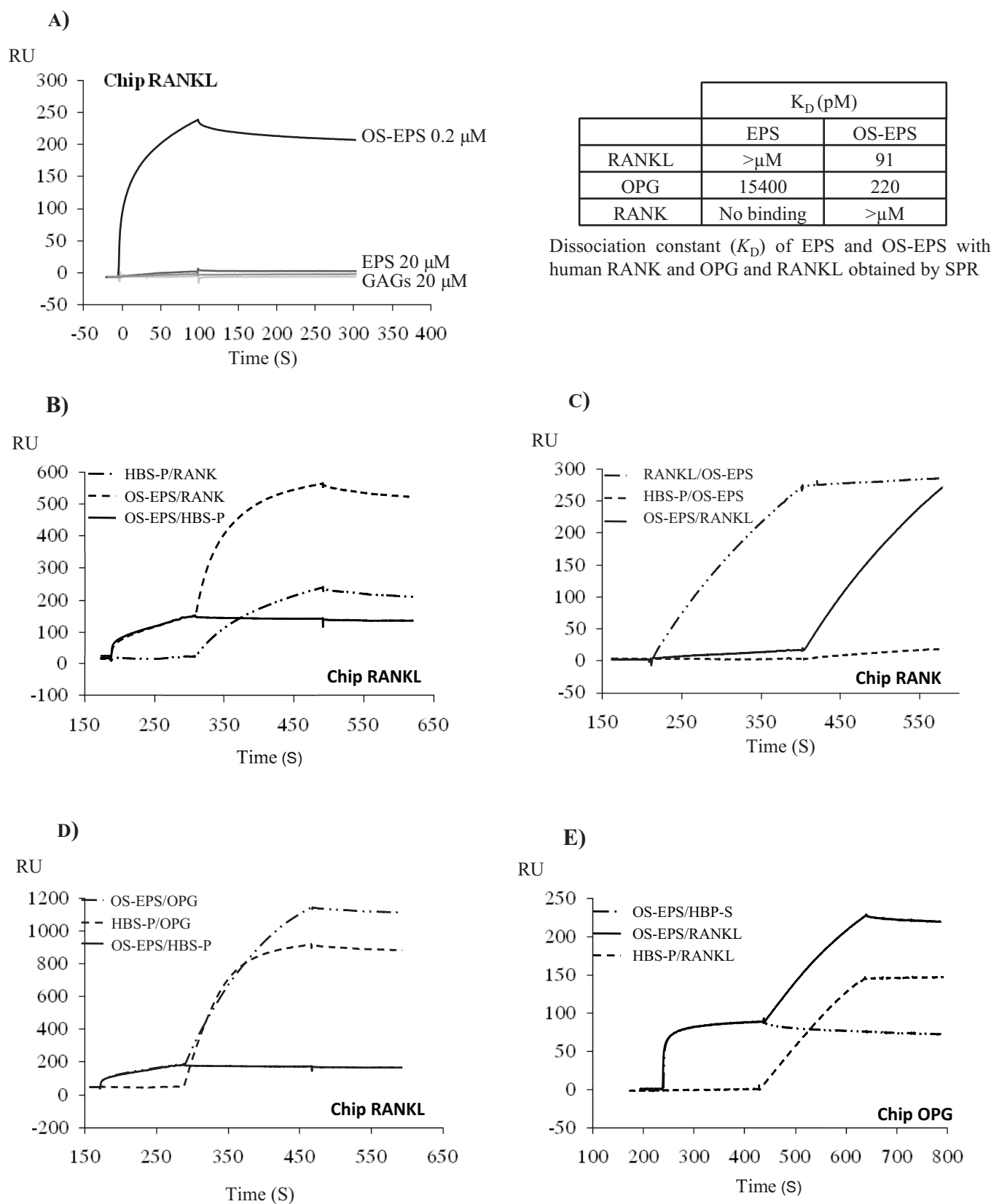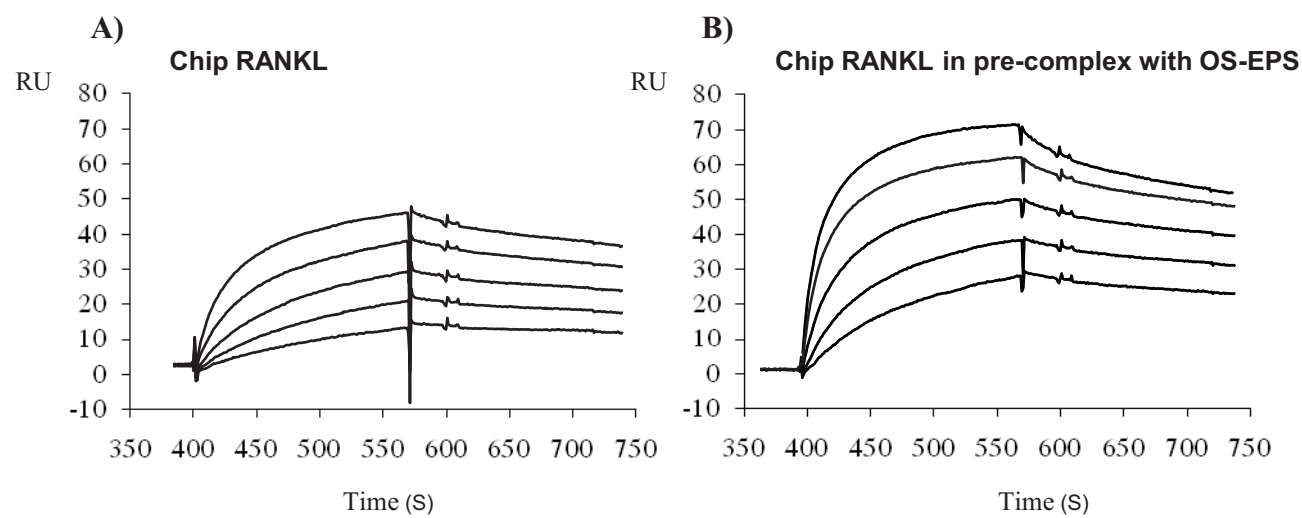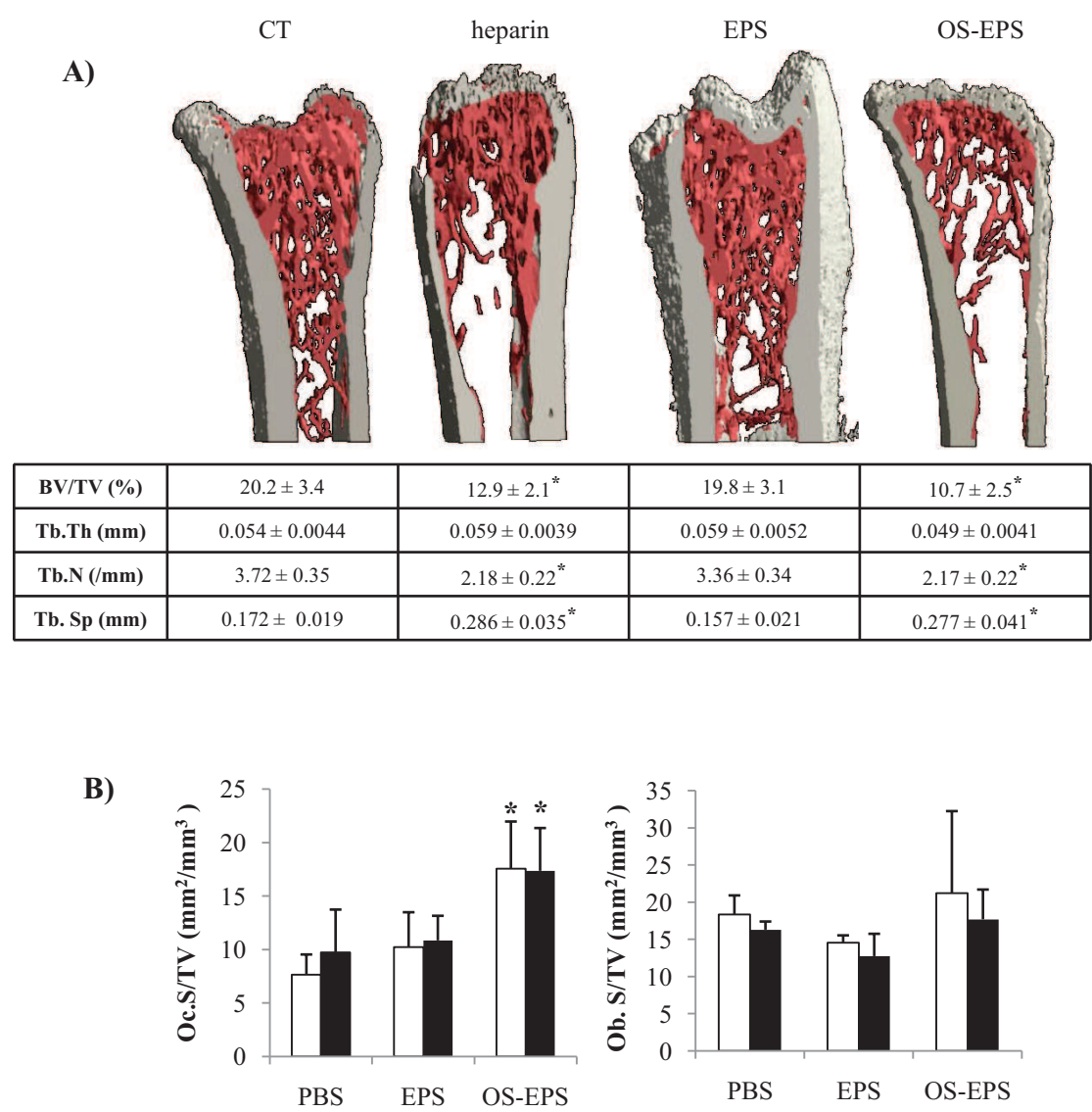|	CT	heparin	EPS	OS-EPS
BV/TV (%)	20.2 ± 3.4	$12.9 \pm 2.1^{*}$	19.8 ± 3.1	$10.7 \pm 2.5^{*}$
Tb.Th (mm)	0.054 ± 0.0044	0.059 ± 0.0039	0.059 ± 0.0052	0.049 ± 0.0041
Tb.N (/mm)	3.72 ± 0.35	$2.18 \pm 0.22^{*}$	3.36 ± 0.34	$2.17 \pm 0.22^{*}$
Tb. Sp (mm)	0.172 ± 0.019	$0.286 \pm 0.035^{*}$	0.157 ± 0.021	$0.277 \pm 0.041^{*}$

B)

Effects of a sulphated 'heparin-like' exopolysaccharide produced

by *Altermonas infernus* on bone biology.

Authors: C. Ruiz Velasco[a,b], M. Baud'huin[a,b], C. Sinquin [c], M. Maillasson[d], D. Heymann[a,b,e], S. Colliec-Jouault[c], M. Padrines[a,b*].

[a] INSERM, U957, Nantes, F-44035, France

[b] Université de Nantes, Nantes Atlantique Universités, Laboratoire de Physiopathologie de la Résorption Osseuse et Thérapie des Tumeurs Osseuses Primitives, EA3822, Nantes, F-44035 France

[c] Laboratoire de Biotechnologie et Molécules Marines, Département Biotechnologies Marines, BIOMAR., IFREMER, Nantes F-44311, France

[d] INSERM U892 and IFR26- Ouest genopole, F-44035 France

[e] Centre Hospitalier Universitaire de Nantes, France

[*] **Corresponding author:**
Dr M. Padrines
EA 3822 - INSERM U957
Faculté de Médecine, 1 rue Gaston Veil
44035 Nantes cedex 01, France
Tel : 33 240 412 846 ; Fax : 33 240 412 860
E-mail : marc.padrines@univ-nantes.fr

1

Key words

Abstract

The growth and differentiation of bone cells is controlled by various factors which can be modulated by heparan sulphates. Here, we investigated the effects of an oversulphated "heparin-like" exopolysaccharide (OS-EPS) on bone. We compared the effect of this compound with that of a native exopolysaccharide (EPS). Long-term administration of OS-EPS causes cancellous bone loss in mice due, in part, to an increase in the number of osteoclasts lining the trabecular bone surface. No significant difference in cancellous bone volume was found between EPS-treated mice and age-matched control mice, underlying the importance of sulphatation in trabecular bone loss. However, the mechanism sustaining this osteoporosis was unclear. To clarify OS-EPS activities, we investigated the effect of OS-EPS in osteogenesis. Our results demonstrated that OS-EPS inhibited osteoclastogenesis in two cell models. By surface plasmon resonance technique we revealed that OS-EPS can constitute a hetero-molecular complex OS-EPS/RANKL/RANK and that RANK had a higher affinity for RANKL pre-incubated with OS-EPS than for RANKL alone which would be in favour of an increase in bone resorption. However, *in vitro*, OS-EPS inhibit the early steps of osteoclast precursor adhesion and therefore inhibits the step of cell fusion. In addition, we showed that OS-EPS reduces the proliferation and accelerates osteoblastic differentiation, leading to strong inhibition of mineralized nodule formation, which would be in favour of an increase in bone resorption. Taken together, these data show different levels of bone resorption regulation by exopolysaccharides, most of them leading to proresorptive effects.

Introduction

Bone, a specialized connective tissue, is continually remodelled according to physiological events. This remodelling results from the activities of many cell lineages including mainly osteoblasts, osteocytes and osteoclasts. Their cellular interactions control their cellular activities and the bone remodelling intensity. These interactions can be established either through a cell–cell contact or by the release of many polypeptidic factors and/or their soluble receptor chains (cytokines, growth factors). These factors can act directly on osteogenic cells and their precursors to control differentiation, formation and functions (e.g. matrix formation, mineralization, resorption) (Kwan Tat *et al*., 2004). Among these factors, proteoglycans (PGs) appear critical for maintaining an appropriate number of osteoblasts and osteoclasts by modulating their proliferation and/or differentiation (Lamoureux *et al*., 2007).

PGs are composed of a core protein with covalently attached glycosaminoglycan (GAG) chains. These GAGs, linear polymers of repeated disaccharidic units, are sulphated and the number and position of sulphate are extremely variable in sulphated GAG depending on the tissular, cellular, and metabolic context, ensuring structural variability of these polysaccharides (Bernfield, 1999). These PGs are ubiquitous, being present as cell surface molecules anchored in the plasma membrane, as components of the insoluble extracellular matrix or as soluble molecules present in extracellular matrix and serum. PGs function in both cell–cell and cell–extracellular matrix adhesion and can also act to promote assembly of extracellular matrix molecules. Additionally, PGs bind a wide range of bioactive molecules, such as growth factors, chemokines, which regulate cell behaviour in normal and pathological processes. Thus, PGs or GAGs associated to the cell membrane or resident in the extracellular bone matrix regulated the bone growth and remodelling (Ruiz Velasco *et al*., 2010).

The osteoprotegerin (OPG)/Receptor Activator of NF-κB (RANK)/RANK Ligand (RANKL) molecular triad has been identified as members of a ligand-receptor system that directly regulates osteoclast differentiation and osteolysis (Simonet *et al*, 1997). While RANKL is a powerful inducer of bone resorption through its interaction with RANK (Kong *et al*., 1999), OPG acts as a decoy receptor for RANKL, thereby strongly inhibiting osteoclast differentiation (Yasuda *et al*., 1998). Any dysregulation of their respective expression leads to pathological conditions (Wittrant *et al*., 2004). OPG contains a heparin-binding domain and strongly bind to GAGs with a high affinity (K_D: 0.28 nM for heparin) (Theoleyre *et al*., 2006). Therefore, PGs decrease the bioavailability of OPG inducing its internalization (Standal *et al*., 2002, Kwan Tat *et al*., 2006) are involved in OPG-induced chemotaxis of monocytes (Mosheimer *et al*., 2005) and enhance the RANKL half-life at the cell membrane (Kwan Tat *et al*., 2006). Similarly to OPG, PGs interact with RANKL. For example, Shinmyouzu *et al*. (2007) showed that dermatan sulphate inhibits the binding of RANK to RANKL and reduce the RANKL-induced levels of MAPK signal transduction in osteoclast progenitors, thus abolishing osteoclastogenesis. These data demonstrate that PGs must be considered as essential co-factors modulating bone remodelling. Thus, PGs are not simply passive structural components of cells and extracellular matrices, rather, they are multifunctional molecules that regulate cell behaviour by fine tuning the function of many regulatory proteins (Lamoureux, 2009).

Heparin demonstrates several kinds of biological activities by binding to various extracellular molecules and plays pivotal roles in bone metabolism. However, the role of heparin in the biological activity of bone remains unclear. Recently, Ariyoshi *et al.* (2008) showed that heparin, after binding to RANKL, suppressed osteoclastogenesis and inhibited the formation of resorption pits induced by RANKL, whereas the other GAGs showed no effects. In contrast, Irie *et al.* (2007) showed that heparin specifically binds to OPG and

prevents OPG-mediated inhibition of osteoclastic bone resorption in the coculture of mouse bone marrow cells and osteoblasts and demonstrated that heparin enhances osteoclastic bone resorption by inhibiting OPG activity. Long-term heparin treatment causes cancellous bone loss in rats due in part to an increase in the number of osteoclasts lining the trabecular bone surface. However, results from various other groups suggest that GAGs, and in particular heparan sulphate (HS) and heparin, are potent co-stimulators of osteogenic signaling pathways (Zhao et al, 2006; Jackson et al, 2007; Ling et al, 2010)). Thus, the opportunity arises to leverage the stimulatory properties of HS-derived compounds as adjuvants for osteo-inductive therapies.

A broad series of polysaccharides has emerged as an important class of bioactive products (Franz and Alban, 1995; Bernas, 2003; Mayer and Lehmann, 2001). Polysaccharide-producing marine microorganisms occur widely in nature in different types of habitat (Sutherland, 1996), and some thermophilic and mesophilic polysaccharide-producing strains have been isolated from deep-sea hydrothermal vents (Guezennec, 2002; Nichols et al., 2005). *Alteromonas infernus,* classified as a non-pathogenic microorganism by the Institut Pasteur, secretes a water-soluble acidic heteropolysaccharide (Raguénès et al., 1997). The composition of this high-molecular-weight polysaccharide (10^6 g/mol) differs in monosaccharide content and/or ratio and sulphate content (10%) from other polysaccharides isolated from deep-sea hydrothermal bacteria and from polysaccharides of other origins. Structural characterization has shown that this exopolysaccharide is a highly branched acidic heteropolysaccharide composed of neutral sugars (glucose, galactose) and uronic acids (glucuronic acid and galacturonic acid) (Roger et al, 2004). The high-molecular-weight exopolysaccharide was chemically depolymerised and sulphated, with a view to obtaining a bioactive compound compatible with a therapeutic use (Roger et al, 2004). Highly sulphated low molecular-weight exopolysaccharide (40% sulphate groups, MW: 24 000, Fig. 1), with

uronic acid and sulphate contents comparable to those of heparin, were obtained without altering the osidic composition of this polymer (Guezennec *et al*., 1998). In contrast to the exopolysaccharide secreted by *Alteromonas infernus*, this oversulphated exopolysaccharide (OS-EPS) exhibits anticoagulant properties. It is less potent than low-molecular-weight heparin and unfractionated heparin (2.5 and 6.5 times, respectively), and should therefore carry a lower risk of bleeding (Colliec-Jouault *et al*., 2001). OS-EPS increases angiogenic properties of FGF-2 (Fibroblast growth factors-2) or VEGF (Vascular endothelial growth factor**)**, i.e. endothelial cell proliferation and differentiation into vascular tubes; however it also inhibits the effect of FGF-2-induced cell migration (Matou *et al.*, 2005). These angiogenic properties of OS-EPS are related to its sulphate content because no effect was observed with the native low molecular-weight exopolysaccharide (EPS). FGFs play an important major role in the control of cell proliferation, differentiation, and survival in several tissues including bone (Marie, 2003). Notably, FGF2 was found to promote cell growth and osteoblast differentiation in bone marrow-derived mesenchymal cells (Miraoui *et al*, 2009). In addition, FGF2 upregulate the expression of RANKL on rheumatoid arthritis synovial fibroblasts (Nakano *et al.*, 2004). However, no data concerning the structure and biological activity of these exopolysaccharides on bone cells proliferation and differentiation were available until now. To explore its capacity to promote bone resorption or formation, an influence of OS-EPS on bone cell proliferation and differentiation was determined. OE-EPS was compared with EPS in order to study the effect of sulphate content on the biological properties of the exopolysaccharide.

Results

OS-EPS inhibits the proliferation of BMSCs during osteoblastic differentiation

To study the effect of OS-EPS on osteoblast precursors, we used the bone marrow stem cells (BMSCs) model, in which dexamethasone is known to induce osteoblast differentiation. Proliferation of BMSCs during osteoblastic differentiation was analyzed in the presence of OS-EPS. 25 µg/mL of OS-EPS significantly inhibited cell proliferation (Fig. 2A and 2B) in contrast to EPS. To determine whether these effects were due to inhibition of cell proliferation and/or induction of cell death, we used time-lapse microscopy to monitor the mitosis events. The results demonstrated a 70% inhibition of cell mitosis in the presence of 25µg/mL of OS-EPS after 48 h of culture as compared to the control (Fig. 2C). To determine whether the OS-EPS induced death in BMSCs by apoptosis, Hoechst staining and caspase-3 activation were investigated. Hoechst staining showed no modification of nuclear morphology in the presence of OS-EPS as compared to control cells (data not shown). Concerning the caspase-3 activity in BMSCs, the results showed that OS-EPS does not induce any activation of caspases (not shown). Flow cytometry of DNA content was performed to identify cell cycle perturbations following treatment with OS-EPS over a 48-h period in BMSCs. Although 24 h of OS-EPS treatment did not modulate the cell cycle in BMSCs (data not shown), 48 h of OS-EPS treatment induced a cell cycle arrest in G1 phases (Fig. 2D). Indeed, the number of cells in G1 phases increased from 73 ± 2 to 83 ± 3 % when treated with OS-EPS (Fig. 2D). This observation was concomitant with a reduction of cells in S and G2/M phases: 25 ± 3 versus 17 ± 2 % (Fig. 2D). EPS had no effect in any of the experimental conditions, underlying the importance of sulphatation in the proliferation.

OS-EPS inhibits mineralized nodule formation in pre-osteoblasts

To examine the role of OS-EPS on extracellular matrix mineralization in BMSCs cultures, BMSCs were treated for 17 days with OS-EPS, after which mineral was visualized by von Kossa staining. As demonstrated in Fig. 3A, OS-EPS dose-dependently inhibited mineralization with maximal inhibition occurring at 50 µg/mL. In late BMSCs culture, OS-EPS reduced the formation of bone nodules. To further understand the mechanism by which OS-EPS inhibits mineralization, cultures were treated with 25 µg/mL OS-EPS during days 3–17. OS-EPS reduced the formation of bone nodules when added in the two first weeks but not later (Fig. 3B), suggesting that OS-EPS blocks culture mineralization mainly by adversely affecting osteoblast differentiation and matrix deposition during the early matrix assembly stage and not by direct binding to hydroxyapatite crystals during the mineralization stage. Based on reduced mineralization, it was expected that OS-EPS would reduce expression of osteoblastic markers in cells. This study was performed on BMSCs under conditions where runt-related transcription factor 2 (Runx2), alkaline phosphatase (ALP) and type I collagen expression (Col1α1) were observed by preosteoblast stage, followed by bone sialoprotein (BSP) and osteocalcin (OC) by mature osteoblast stage. Unexpectedly, after 17 days of treatment, OS-EPS induced BSP and OC in a dose dependent manner (Fig. 3C). In contrast, OS-EPS reduced ALP, Runx2 and colα1 mRNA level in a dose dependent manner (Fig. 3C). However, Runx2 was transiently and strongly induced by OS-EPS; it increased after 7 days, reached a peak level at 10 days (14 days for the control), and decreased thereafter (Fig 3 C). This result clearly demonstrated an effect of OS-EPS on the osteoblastic differentiation. OS-EPS acted at the early steps of the process by affecting the preosteoblast and accelerating the osteoblactic differentiation.

OS-EPS inhibits RANKL-induced osteoclastogenesis in human models

CD14$^+$ cells are human monocyte cells which can differentiate into tartrate-resistant acid phosphatase (TRAP)-positive multinucleated cells in 21 days upon RANKL stimulation. As shown in figure 4A, in contrast to EPS, addition of 0,5µg/ml OS-EPS, at the same time that RANKL addition, almost completely inhibited RANKL-induced osteoclastogenesis (p<0.01). We confirmed this effect in a second model of osteoclastogenesis. RAW 264.7 cells are murine monocyte/macrophage cells which can differentiate into TRAP-positive multinucleated cells in 5 days upon RANKL stimulation. OS-EPS completely inhibited RANKL-induced osteoclastogenesis of RAW 264.7 (results not shown). To better characterize the mechanisms by which OS-EPS inhibits osteoclast formation, the effect of OS-EPS were assessed at different times of the culture period. When OS-EPS was added 3 days before RANKL (D-3) to the culture, no osteoclasts were generated after 17 days (Fig. 4A) and the number of adherent CD14$^+$ osteoclast precursors was decreased compared to the control condition. To determine whether these effects were due to induction of loss of adhesion, the effects of OS-EPS were evaluated by counting viable cells, as assessed by trypan blue exclusion. After the adherence of CD14$^+$ cells in the wells, these cells were incubated with EPS or OS-EPS during 5 days. Blue trypan counting revealed that OS-EPS causes a loss of adherence of this type of cells (Fig. 4B). Thus in this culture condition, fewer osteoclast precursors adhered to the plastic surface and less osteoclasts were generated in the presence of RANKL. The addition of OS-EPS after one week culture step (D7) did not completely inhibit osteoclast formation (Figure 4A). OS-EPS acted at two distinct levels of osteoclastogenesis: i) at the early steps of the process by affecting and decreasing cell adherence and ii) at the end of the osteoclastogenesis process by inhibiting the spreading of the preformed osteoclasts. This result clearly demonstrated an effect of OS-EPS on RANKL-induced osteoclastogenesis. OS-EPS acted at the early steps of the process by affecting and decreasing cell adherence.

OS-EPS binds to RANKL

OPG/RANK and RANKL have been identified as members of a ligand-receptor system that directly regulates osteoclast differentiation and osteolysis. While RANKL is a powerful inducer of bone resorption through its interaction with RANK, OPG is a soluble decoy receptor and acts as a strong inhibitor of osteoclastic differentiation.

Surface plasmon resonance (SPR)-binding assays showed that recombinant full length OPG binds immobilized heparin (Theoleyre *et al.*, 2006). To determine the involvement of OS-EPS in the binding of OPG, we determined kinetic parameters by injecting different concentrations of OS-EPS over immobilized OPG and thus demonstrated a high-affinity OPG binding to OS-EPS (dissociation constant K_D: 0.22 nM) (Fig. 5). To explore the molecular mechanism underlying the effect of OS-EPS on RANKL-induced osteoclastogenesis, we investigated the molecular interactions between RANKL and OS-EPS by SPR. Surprisingly, OS-EPS was also able to bind to immobilized-RANKL, whereas EPS was not (Fig. 5A). We next compared OS-EPS activity to that of heparin, heparan sulphate, chondroitin sulphate and dermatan sulphate. None of the GAGs analyzed were able to bind to RANKL, with the exception of OS-EPS (Fig. 5A). Furthermore, using a single cycle kinetic assay, the K_D of OS-EPS for RANKL was 91 pM (Fig. 5).

Since RANKL is the natural ligand of RANK, we wondered whether OS-EPS could inhibit the complex RANKL–RANK present at the osteoclast membrane. We investigated the molecular interactions between OS-EPS, RANKL and RANK by SPR technique. We confirmed that RANK or RANKL bound to immobilized RANKL or immobilized RANK, respectively (Fig. 5B and 5C). While, in our conditions, OS-EPS did not bind to immobilized RANK (Fig. 5C), it bound to the preformed RANKL/RANK complex (Fig. 5B) thereby forming a ternary complex OS-EPS/RANKL/RANK. In addition, the pre-incubation of OS-

EPS (30 min at room temperature) with RANK or RANKL did not inhibit the capacity of OS-EPS to further bind to the preformed ternary complex OS-EPS/RANKL/RANK (data not shown). However, sensorgrams with RANKL, pre-incubated or not with OS-EPS, immobilized on the surface of a CM5 sensor chip revealed different binding response units for RANK (Fig. 5B). To determine the biophysical binding parameters for the ternary complex interactions, real-time SPR spectroscopy was performed (Fig. 6). Surprisingly, the kinetic study shows a significant increase of the association rate of RANK to RANKL pre-incubated with OS-EPS facilitating the complex formation. RANK had higher affinity for RANKL pre-incubated with OS-EPS surface sensor chips than for RANKL surface sensor chips (> 2-fold). This result would be in favour of an increase in bone resorption which has not been observed during the study of osteoclastogenesis (Fig. 4).

RANKL is not only a ligand for RANK but also acts as ligand for the decoy receptor OPG. To determine whether or not OS-EPS could affect the complex OPG/RANKL, RANKL has been immobilized on a sensor chip, and the capacity of OS-EPS to bind to complex OPG/RANKL was analyzed. Similar to the RANKL/RANK complex, OS-EPS is able to bind to a preformed OPG–RANKL complex (Fig. 5D and 5E) forming another ternary complex OS-EPS/RANKL/OPG. Also, the pre-incubation of OS-EPS (30 min at room temperature) with OPG or RANKL did not inhibit the capacity of OS-EPS to further bind to the preformed ternary complex OS-EPS/RANKL/OPG (data not shown). However, no modification of the kinetic parameters of the interaction of the OPG to RANKL pre-incubated with OS-EPS was observed.

OS-EPS induces trabecular bone loss.

During the 28 days of this study all of the mice from the different treatment groups (OS-EPS, EPS and heparin-treated) gained weight. No significant differences with respect to

weight gain were found between those mice treated with either OS-EPS or EPS or heparin or age-matched controls. However, at the femur level, micro-CT scanner analysis revealed that the mouse femur was characterized by large remodelling activities as compared to control femurs (Fig.7A). Thus, OS-EPS produced a reduction in cancellous bone volume when compared with control. The effect of OS-EPS on cancellous bone was similar to that of our positive control (heparin). OS-EPS did not modify the cortical bone volume (data not shown) but significantly reduced the trabecular bone volume ($p< 0.01$; Fig.7A). The trabecular number (Tb.N) was significantly reduced by OS-EPS ($p<0.05$), whereas the trabecular space (Tb.Sp) increased ($p<0.05$). Trabecular thickness (Tb.Th) was not significantly altered (Fig. 7). However, no significant difference in cancellous bone volume (BV/TV) was found between EPS-treated mice and age-matched control mice, underlying the importance of sulphatation in trabecular bone loss.

Histologic sections were stained with TRAP or ALP to quantify osteoclast or osteoblast surface-based data, respectively. Figure 7B shows that the parameter of osteoblast surface was not significantly different when comparing OS-EPS or EPS-treated mice and age-matched controls. In contrast, OS-EPS produced an increase in the percentage of cancellous bone covered by osteoclasts. Whereas mice given 6 mg/kg OS-EPS showed a 125% ± 23% ($p<0.05$) increase in osteoclast surface, osteoclast surface was unaffected by treatment with EPS (Fig. 7B).

Discussion

In the present study, we have shown that long-term administration of OS-EPS, a `heparin-like' component (containing uronic acid and sulphate contents comparable to those of heparin) with `heparin-like' activity (anticoagulant properties), causes cancellous bone loss in mice due, in part, to an increase in the number of osteoclasts lining the trabecular bone surface. Our results are therefore similar to results published many years ago, in which long-term administration of heparin was shown to lead to the development of osteoporosis (Muir *et al.*, 1996). Similarly, Barbour *et al.* (1994) showed that 36% of pregnant women undergoing long-term heparin treatment had a 10% reduction in femoral bone mineral density. Both heparin (Muir *et al.*, 1996; Muir *et al.*, 1997, Rajgopal *et al.*, 2008) and OS-EPS increase the process of bone resorption. Although, heparin and OS-EPS has similar effects on osteoclast number, heparin was found to decrease osteoblast number (Muir *et al.*, 1996; Muir *et al.*, 1997, Rajgopal *et al*., 2008), whereas OS-EPS has no effect. These effects resulting in bone loss begin early in the course of OS-EPS treatment (data not shown). However, the mechanism sustaining osteoporosis was unclear and it was difficult to determine if these effects on bone resorption were due to the direct effect of OS-EPS on osteoclasts or indirectly *via* its osteoblast activity.

GAGs exhibit several kinds of biological activities by binding to various extracellular molecules and play a pivotal roles in bone metabolism. An indirect proof of heparan sulphate proteoglycans (HSPGs) involvement in osteoclast functions was recently shown in a publication that demonstrated that heparanase, a HS-degrading endoglycosidase expressed in osteoblastic cells, stimulates bone formation and bone mass (Kram *et al.*, 2006). The effect of GAGs on osteoclastogenesis is controversial. For example, Ariyoshi *et al.* (2008) and Shinmyouzu *et al.* (2007) showed an inhibition of osteoclastogenesis after a direct interaction

of GAGs with RANKL. In contrast, Irie *et al.* (2007) showed a stimulation of osteoclastic bone resorption by inhibiting OPG activity. Our results clearly demonstrated that OS-EPS inhibited osteoclastogenesis in two systems tested. Furthermore, we demonstrated the importance of the sulphation of the exopolysaccharide in their inhibitory effect. Sulphation also plays a key role in GAGs biological activities as revealed by the present work. Sulphated polysaccharides enhance the biological activity of both homodimers and heterodimers of bone morphogenetic protein (BMP) by continuously serving the ligands to their signalling receptors expressed on cell membranes, similar to oversulphated chondroitine sulphate that binds to BMP-4 and enhances osteoblast differentiation (Miyazaki *et al.*, 2008). Sulphation has clearly been shown to participate in to the control of cell biology. Kumarasuriyar *et al.* (2009) showed that the chlorate-induced-desulphation of GAGs expressed by MG63 cells delayed *in vitro* osteogenesis. In addition, sulphation strongly modulates the interaction of GAGs with proteins such as growth factors or enzymes (Lamoureux *et al.*, 2007; Gallagher, 2006).

However, the question remains of how we can explain the strong discrepancies between the *in vivo* and *in vitro* results. In this context, we first analyzed the interaction of OS-EPS with the OPG/RANK/RANKL molecular triad and the effect of OS-EPS on adhesion of osteoclast precursors. Here, we clearly showed that OS-EPS can constitute a hetero-molecular complex (OS-EPS /RANKL/RANK or OS-EPS/RANKL/OPG) as demonstrated by surface plasmon resonance technique and that RANK possesses a higher affinity for RANKL pre-incubated with OS-EPS than for RANKL alone. Contrarily, OS-EPS does not interfere in the binding of RANKL by OPG. These results also revealed that RANKL had higher affinity for OS-EPS (K_D = 91 pM) than for OPG (K_D = 0.27 nM, Kwan Tat *et al*, 2006). In conclusion, the preferential binding of RANKL to OS-EPS is able to facilitate the binary OS-EPS/RANKL complex formation, which, in turn, may facilitate the ternary OS-EPS/RANKL/RANK complex formation, which would be in favour of an increase of the bone

resorption. Secondly, we analyzed the effects of OS-EPS on adhesion of osteoclast precursors, demonstrating a sequential effect of OS-EPS on RANKL-induced osteoclastogenesis. OS-EPS inhibit the early step of osteoclast precursor adhesion and consequently inhibits the step of cell fusion. The alteration of cell adhesion and morphology prevents the cell fusion of osteoclast precursors and blocks osteoclast resorption which is particularly sensitive to cell morphology to develop their brush border (Rousselle and Heymann, 2002).

Our data are in favour of a direct inhibitory activity of OS-EPS on osteoclastogenesis and the effect observed *in vivo* may be explained by its effects on the bone osteoblast compartment and then by the dysregulation of the balance between osteoblasts and osteoclasts or by a slow-down of bone remodeling. The rate of bone formation is dependent on the commitment and replication of osteoprogenitor cells, their differentiation into functional osteoblasts and the life span of mature osteoblasts. Cells are committed to the osteoblast lineage by induction of the transcription factor Runx2 (Karsenty, 2001). This osteoblast differentiation is regulated by the actions of systemic and local signalling factors. Among these factors are FGFs, a family of polypeptides that control the proliferation and differentiation of osteoblast cell (Xiao *et al*., 2010). Thus, FGF2 is a powerful promoter of bone growth, enhancing mineralized nodule formation (Downey *et al*., 2009). This effect is mediated via HSPGs that coordinate the interaction of FGFs with their high-affinity tyrosine kinase receptors, the FGFRs (Eswarakumar *et al*., 2005). The interaction of PGs with FGFs provides a physiological mechanism for regulation of FGF signalling, FGFR1, and the extracellular signal-regulated kinase pathway. Furthermore, osteoclast differentiation and activity are regulated by GAGs at different levels, as revealed in previous studies. FGF-2 induces, after the binding to HS, the expression of RANKL and osteoclast maturation by rheumatoid synovial fibroblasts. FGF-2 not only augments the proliferation of rheumatoid synovial fibroblasts, but is also involved in osteoclast maturation, which leads to bone

destruction in rheumatoid arthritis (Nakano *et al.*, 2004 Matou *et al.* (2005) showed the binding of OS-EPS to FGF-2, therefore we hypothesize that FGF-2 can induce bone resorption after binding to OS-EPS.

Osteoblastic cells produce a complex extracellular matrix composed of a mixture of PGs, collagens and non-collagenous proteins. The interaction of PGs with matrix effector macromolecules via either their GAG chains or their protein core is critical in regulating a variety of cellular events. Alterations in the structural composition of the GAG/PG components of the extracellular matrix may have important consequences on cell proliferation and/or differentiation. Recently, Haupt *et al*. (2009) demonstrated the dependence of osteogenesis on specific HS chains, in particular those associated with glypican-3. The differentiating osteoblast-committed cells produce a homogenous HS species, which correlates with an increase in the HSPG glypican-3. Abrogation of glypican-3 reduces the expression of the osteogenic transcription factor Runx2. The data demonstrate tight linkage between HS modification and progression of osteogenic precursors through their developmental program.

Our results showed that (1) OS-EPS reduces expression of ALP, collαI, Runx2 (preosteoblast stage) in BMSCs cells and enhances OC and BSP mature osteoblast stage); (2) exogenous application of OS-EPS to cultures of primary BMSCs during *in vitro* differentiation completely blocks BMSC mineralization; (3) OS-EPS strongly reduces the proliferation of differentiating osteoblasts BMSCs cells. This proliferation inhibition was not due to an induction of apoptosis. These results suggest that OS-EPS reduces the proliferation and accelerates the osteoblastic differentiation, leading to strong inhibition of mineralized nodule formation that would be in favour of an increase of the bone resorption. However, these results cannot explain the effect observed *in vivo*. No significant difference in obsteoblast surface was found between OS-EPS-treated mice and age-matched control mice.

17

Although the explanation for these conflicting results is unclear, findings in a whole bone organ culture system are more likely to reflect events *in vivo* than those that occur in isolated osteoblast cultures. It is possible that this reflects the propensity of OS-EPS to bind to other critical growth factors, such as (1) bone morphogenetic protein (BMP). HS and chondroitine sulphate directly regulate the BMP-mediated differentiation of mesenchymal stem cells (hMSCs) into osteoblasts. BMPs, which have been shown to be heparin-binding proteins, induce osteoblast differentiation in hMSCs (Manton *et al.*, 2007). The role of heparin in the biological activity of BMP remains unclear. Heparin inhibits the binding of BMP-2 to BMPR and subsequent mRNA expression of Runx2, as well as phosphorylation of Smad and MAPK signal transduction. Furthermore, heparin was found to suppress the differentiation of osteoblastic MC3T3-E1 cells treated with BMP-2 (Kanzaki *et al*., 2008). In contrast, Zhao et al (2006) showed that heparin enhances BMP-induced osteoblast differentiation by protecting BMPs from degradation and inhibition by BMP antagonists; (2) tumor growth factorβ1 (TGFβ1), a known inhibitor of osteoprogenitor growth, which has a higher affinity than several other bone-related, heparin-binding growth factors (Manton *et al.*, 2006). This binding suggests that GAGs play a critical role in regulating TGF-β availability. Overcoming such sugar-mediated inhibition may prove important for wound repair. Given the importance of "heparin like" exopolysaccaharide for bone metabolism, it can be anticipated that OS-EPS due to its structural similarity with HS chains somehow interferes with the biological activities of these cell surface- and extracellular matrix-associated molecules. Taken together, these data show different levels of bone resorption regulation by GAGs or exopolysaccharides, most of them leading to proresorptive effects.

Materials and methods

Materials. Human M-CSF, human RANK and human OPG were obtained from R&D Systems (Abington, UK). Human RANKL was kindly provided by Amgen Inc. (Thousand Oaks, USA). Heparin sodium salt, heparan sulphate from bovine kidney, heparan sulphate from porcine intestinal mucosa, chondroitin sulphate from shark cartilage, dermatan sulphate from porcine intestinal mucosa and hyaluronic acid were purchased from Sigma (St Quentin Fallavier, France).

The two low molecular weight exopolysaccharides (EPS and OS-EPS) were obtained from high molecular weight exopolysaccharide by previously described procedures (Colliec-Jouault et al., 2001; Guezennec et al., 1998; Raguennes et al., 1997). EPS and OS-EPS are homogenous fractions with an average molecular mass of 13 kDa and 24 kDa, and 10% and 40% sulphate groups, respectively, as determined by analytical high performance size-exclusion chromatography (Colliec-Jouault et al., 2001).

Culture medium and preparation of BMSCs. BMSCs were isolated from the bone marrow of 4 week-old Sprague-Dawley rats (Janvier, Le Genest Saint Isle, France). After anesthetization and cervical dislocation, femurs and tibias were dissected aseptically and cleaned of soft tissues. BMSCs were then flushed out with a syringe fitted with a 22-gauge needle containing maintenance media (MM) consisting of α-Minimal Essential Medium (α-MEM, Invitrogen) supplemented with 10% fetal calf serum (FCS) and 1% antibiotics (100 U/mL penicillin and 100 mg/L streptomycin). After centrifugation (5 minutes at 1600 rpm) cells were resuspended in 20 mL of MM. For osteogenic media (OM) culture conditions, this media was supplemented with 50 μg/mL ascorbic acid (Sigma) and 10^{-8} M dexamethasone (Sigma). Cells between passages 0 and 3 were used for all experiments. Cells were maintained at 37°C in a humidified atmosphere containing 5% CO_2.

Proliferation of BMSCs. Cells were plated (5×10^4/well) into a 6-well plate in MM overnight. Then MM was replaced by fresh OM in the presence or absence of 25 µg/mL EPS or OS-EPS, and cells were left to recover for 7 days (media was changed every 3 days). Then, cells in each well were washed three times in 1x Dulbecco phosphate-buffered saline (DPBS), trypsinized and counted in triplicate at day 3 and 7 by using blue trypan exclusion dye.

Induction of apoptosis. Programmed cell death was monitored microscopically following Hoechst staining. BMSCs were seeded at 10^4 cells/well in a 24-well plate and cultured for 24 h in MM. Then MM was replaced by fresh OM in the presence of 25 µg/mL OS-EPS for 24, 48, and 72 h or 100 nM staurosporine (Sigma) for 16 h as a positive control. At the end of the culture period, cells were stained with 10 µg/ml Hoechst reagent for 30 min at 37°C, and then observed under UV microscopy (DMRXA; Leica, Wetzlar, Germany).

Induction of apoptosis was also investigated by cleavage of caspase-3 substrates in supernatants of cultures with or without OS-EPS treatment. BMSCs were seeded at 15×10^3 cells/well (in a 24-well plate), then incubated with OS-EPS (25 µg/mL) for 24, 48, and 72 h. Cells incubated with 1 µM staurosporine for 6 h were used as positive controls. At the end of the incubation period, the cells were lysed with 50 µl of RIPA buffer for 30 min. The cells were then scraped off and protein content was quantified in parallel samples using the BCA (bicinchominique acid + Copper II sulphate) assay. Caspase-3 activity was assessed in 10 µl of the cell lysate with the kit CaspACEi Assay System (Fluorometric, Promega, Madison, USA) following the manufacturer's instructions.

Time-lapse microscopy. BMSCs were plated (2×10^3 cells/well) in triplicate into a 24-well plate in MM overnight. Then MM was replaced by fresh OM in the presence or absence of 25 µg/mL EPS or OS-EPS. Immediately post-treatment, the cultured dishes were placed onto a

time-lapse instrument (Leica) designed to capture transmission-phase images every 10 min from multiwell plates. Images were taken and edited using the MetamorphTM software. Cell divisions were then manually scored.

Cell cycle analysis. Cells were plated in triplicate ($2x10^5$/well) into a 6-well plate in MM overnight. Then MM was replaced by fresh OM in the presence or absence of 25 µg/mL EPS or OS-EPS. After 48 h cells were trypsinized and centrifuged at 1600 rpm for 3 min. Cell pellets were fixed in 70% ice-cold ethanol for 30 min and then washed twice in 100µl of DPBS. Cells were incubated in phosphate-citrate buffer at room temperature for 30 min then in DPBS containing 0.12% Triton X-100, 0.12 mM EDTA and 100 µg/ml ribonuclease A at 37ºC for 30 min. Cells were then centrifuged, washed twice and incubated in 50 µg/ml propidium iodide for 20 min at 4°C. Cell cycle distribution was analyzed by flow cytometry F500 (Beckman Coulter France) based on 2N and 4N DNA content using the MultiCycle software.

Mineralization Assay. BMSCs were plated ($3.5x10^6$ cells/well) in duplicate into a 24-multiwell plate in MM. After 24 hours of culture, the supernatant (MM) containing the non-adherent hematopoietic cells was removed. At confluence (72 h later), MM was replaced by OM (media was changed twice a week) in the presence of 25 µg/mL EPS or OS-EPS. After 1 week of culture, OM was supplemented with 10 mM β-glycerophosphate (Sigma) for 2 weeks (media was changed twice a week) in presence or absence of 25 µg/ml EPS or OS-EPS added at different times of the culture period. Then, Alizarin red staining (Alfa Aesar) was used to detect the mineralized nodules formed _in vitro_. Cells were washed in DPBS and fixed in 70% ice-cold ethanol for 1 h. The ethanol was then removed, and the fixed cells were washed three times with distilled water and incubated with alizarin red (40 mM, pH 7.4) for 10 minutes at

room temperature. After staining, excessive dye was washed gently with running water. Calcification deposits typically stained red. All experiments were performed three times.

Osteogenic differentiation Assay. BMSCs were plated (15×10^6 cells/well) into a 6-multiwell plate in MM. After 24 hours of culture, the supernatant (MM) containing the non-adherent hematopoietic cells was removed. At confluence (72 h later), MM was replaced by OM in the presence of 25 µg/mL EPS or OS-EPS (media was changed twice a week). After 1 week of culture, OM was supplemented with 10 mM β-glycerophosphate for 2 weeks (media was changed twice a week). For RT-qPCR analysis, total RNA was isolated from osteogenic culture at different times using the NucleoSpin II kit (Macherey-Nagel). RNA (500 ng) was reversed-transcribed (RT) using ThermoSript System (Invitrogen). cDNA synthesis was performed using total RNA with oligo(dT) at 50°C for 1 h. qPCR was performed in triplicate for each sample by using 5 µl 2x SYBR Green Supermix buffer (Bio-Rad, Marnes la Coquette, France), 1 µl cDNA, 300 nM of each primer, and DEPC H_2O to a final volume of 10 µl. After denaturing of cDNA at 98ºC for 30 sec, amplification and fluorescence determination were carried out in two steps: denaturation at 95ºC for 15 sec, and annealing and extension at 60ºC for 30 sec. The detection of SYBR Green was performed at the process of annealing. The sequence of the primers used in PCR reactions are shown in Table 1. Cyc1 cDNA as internal controls were used to normalize the data to determine the relative expression of the target genes. Polymerase chain reactions were carried out in 96-well plates using the Chromo4 System (Bio-Rad).

Gene	Gene (full name)	Accesion N°	Sequence	(5'→ 3')
ALP	Alkalin phosphatase	NM_013059.1	Forward: Reverse:	aggggcaactccatttttg ttgtaaccaggccccgttg
Runx2	runt-related transcription factor 2	NM_053470.1	Forward: Reverse:	cacagagctattaaagtgacagtgg aacaaactaggtttagagtcatcaagc
BSP	Bone Sialoprotein	NM_012587.2	Forward: Reverse:	cctacttttatcctcctctgaaacg tcgccatctccattttcttc
OC	Osteocalcin	NM_013414.1	Forward: Reverse:	aagcgcatctatggcaccac tcgagtcctggagagtagcc
Collα1	Alpha-1 type I collagen	NM_053304.1	Forward: Reverse:	catgttcagctttgtggacct gcagctgacttcagggatgt
Cyc1	cytochrome c-1	NM_001130491.1	Forward: Reverse:	tgctacacggaggaagaagc atcctcattagggccatcct

Differentiation of human CD14$^+$ cells into osteoclasts. Human peripheral blood mononuclear cells (PBMCs) were isolated by centrifugation over Ficoll gradient (Sigma Chemicals Co., St. Louis, MO). CD14$^+$ cells were magnetically labeled with CD14 Microbeads and positively selected by MACS technology (Miltenyi Biotec, Bergisch Gladbach, Germany). CD14$^+$ cells were plated (45×10^3 cells/well) in triplicate into a 96-well plate in α-MEM containing 10% FCS and 25 ng/ml human M-CSF. After 3 days of culture, media was changed with fresh medium containing 10% FCS, 25 ng/ml human M-CSF, with or without 100 ng/ml hRANKL. Then medium was changed every 4 days. The formation of osteoclasts occurred around 14 days and was observed by tartrate-resistant acid phosphatase (TRAP) staining. In this experiment, EPS or OS-EPS were added at different times of the culture period. Then, multinucleated cells (>3 nuclei) were counted under a light microscope (Leica DM IRB, Nanterre, France; Camera: Olympus D70, Analysis software: Olympus DP Controller/Manager, Hamburg, Germany) after TRAP staining (Sigma, Saint Quentin-Fallavier, France)

Differentiation from the murine RAW 264.7 monocytic cell line. Murine RAW 264.7 monocytic cells (ATCC, Promochem, Molsheim, France) were cultured in phenol red-free α-Minimal Essential Medium (α-MEM) (Invitrogen, Eragny, France) supplemented with 10% fetal calf serum (FCS) (Perbio, Logan, USA) and 1% non essential amino acids (Invitrogen). To induce osteoclast formation, RAW 264.7 cells were scraped then incubated at 37°C for 2 minutes to allow adherence of the more differentiated cells. Non-adherent cells were then seeded in fresh medium at a density of 3×10^3 cells/well in a 96-well plate. After 2 hours of culture, the medium was changed for fresh medium containing 100 ng/ml hRANKL with or without 0,5 µg/ml EPS or OS-EPS. The cells were stained histochemically for TRAP and the number of TRAP-positive multinuclear cells (MNCs) containing 3 or more nuclei was counted.

Adherence *of human CD14$^+$ cells.* Cells were plated (25×10^4 cells/well) in triplicate into a 96-well plate in α-MEM containing 10% FCS and 25 ng/ml human M-CSF during 3 days (time required for these cells to adhere). The medium was then replaced with fresh medium containing α-MEM, 10% FCS and 25 ng/ml human M-CSF in the presence of 1 µg/ml EPS or OS-EPS during 5 days (media were changed once). Then, non-adherent cells in the supernant were counted in triplicate by using blue trypan exclusion dye. The adherent cells were washed three times in DPBS, trypsinized and counted as above.

Surface plasmon resonance-binding assays. Experiments were carried out on a BIAcore 3000 instrument (BIAcore). RANKL, OPG (5 µg/ml in 10 mM acetate buffer, pH 4.0 and pH 5.0 (1:1;v/v)) and RANK (10 µg/ml in 10 mM acetate buffer, pH 5.0) were covalently immobilized to the dextran matrix of a CM5 sensor chip (BIAcore) via its primary amino groups at a flow rate of 30 µl/min. Immobilization levels ranging of 4000 resonance units

(RU) (RANKL and OPG) and 5000 RU (RANK) were obtained. EPS and OS-EPS K_D values for OPG, RANK and RANKL were determined using single cycle kinetics, starting with 1 nM OS-EPS or 100nM EPS (OPG), 250 nM OS-EPS or 2 μM EPS (RANKL) and 100 nM OS-EPS or 2 μM EPS (RANKL), then 1⁄2 dilutions. For binding analysis over the immobilized RANKL, OPG or RANK chip, the concentrations of 1 μg/ml OPG, 2 μg/ml RANK, 0.5 μg/ml RANKL, 20μM GAGs (heparin, or heparan sulphate, or chondroitin sulphate, or dermatan sulphate, or hyaluronic acid), 20 μM EPS and 200 nM OS-EPS were used. Binding assays were performed at 25ºC in 10 mM Hepes buffer, pH 7.4, containing 0.15 M NaCl and 0.005% P20 surfactant (HBS-P buffer, BIAcore) at a flow rate of 30 μl/min. Control sensorgrams (flow cell without RANKL, OPG and RANK) were automatically subtracted from the sensorgrams obtained with immobilized RANKL or OPG or RANK to yield true binding responses. The resulting sensorgrams were fitted using BiaEval 4.1 software (BIAcore).

Animal studies. twenty four 4-week-old male C3H/HeN male mice (Janvier, Le Genest Saint Isle, France) were housed under pathogen-free conditions at the Experimental Therapy Unit (Medicine Faculty of Nantes, France) in accordance with the institutional guidelines of the French Ethical Committee and under the supervision of authorized investigators. After 7 days of acclimatization these animals were assigned randomly to four groups: control (CT), heparin (Sigma H4784, 140U/mg, 50mg/ml), EPS and OS-EPS. All mice received (6 mg/kg) daily s.c. injection for a period of 28 days, consistent with the period of rapid growth in young mice. The 29th day, these animals were anesthetized with isoflurane (0.2% air, delivered via nosecone) and sacrificed by cervical dislocation. Bilateral femurs of each animal were dissected for histological studies and microarchitectural parameter quantification. Two independent experiments were performed.

Histological analysis. After sacrifice, left femur were cleaned from adjacent tissues and fixed in 10% buffered formaldehyde. Then samples were decalcified in 4% EDTA 0.2% paraformaldehyde (pH 7.4) buffer for 4 weeks and embedded in paraffin wax for TRAP and ALP staining. Five-μm-thick sections were cut through the femur (microtome: Leica SM 2500; Leica Instruments GmbH) and mounted on glass slides. Analysis and quantification of osteoblastic and osteoclastic areas were done using a Leica Q500 image analysis system.

Micro-computed tomography (μCT). After sacrifice, the right femur from each animal was dissected of soft tissues, fixed in 10% buffered formaldehyde and the distal metaphysis was used for micro-computed tomography (μ-CT) on a SkyScan-1072 (SkyScan, Aartselaar, Belgium). CT-Analyser software (from SkyScan) was used to analyse the structure of the sample, using the global segmentation method. Two-dimensional (2D) images were used to generate three-dimensional (3D) reconstructions and to calculate morphometric parameters with the SkyScan CtAn 3D creator software supplied with the instrument. Analysis was performed for the trabecular bone, whereby the trabecular region was precisely contoured in each single cross section manually. Bone volume ratio (BV/TV), trabecular thickness (Tb.Th), trabecular number (Tb.N) and trabecular space (Tb.Sp) were assessed.

Statistical analysis. All analyses were performed using GraphPad InStat v3.02 software (La Jolla, CA). The mean ± SD was calculated for all conditions and compared by ANOVA. In vivo experimentation results were analyzed with the unpaired nonparametric Mann–Whitney U test using two-tailed P-values. Differences relative to a probability of two-tailed $p < 0.05$ were considered significant.

Acknowledgments

Abbreviations

GAG : glycosaminoglycan

PG : proteoglycan

OPG : osteoprotegerin

RANK : Receptor Activator of NF-κB

RANKL : RANK Ligand

HS: Heparan Sulphate

EPS: ExoPolySaccharide

OS-EPS : oversulphated EPS

FGF: Fibroblast Growth Factor

VEGF: Vascular Endothelial Growth Factor

BMSC: Bone Marrow Stem Cell

ALP: Alkaline Phosphatase

Collα1: type 1 Collagen

BSP: Bone SialoProtein

OC: Ostéocalcin

SPR: Surface Plasmon Resonance

BMP: Bone Morphometric Protein

TGFβ: Tumor Growth Factor β

References

Ariyoshi W, Takahashi T, Kanno T, Ichimiya H, Shinmyouzu K, Takano H, Koseki T, Nishihara T. 2008. Heparin inhibits osteoclastic differentiation and function. *J. Cell. Biochem.* 103: 1707-1717.

Barbour LA, Kick SD, Steiner JF, LoVerde ME, Heddleston LN, Lear JL, Baron AE, Barton PL. 1994. A prospective study of heparin-induced osteoporosis in pregnancy using bone densitometry. *Am. J. Obstet. Gynecol.* 170 : 862-869.

Bernas GC. 2003. Angiotherapeutics from natural products: from bench to clinics? *Clin Hemorheol Microcirc.* 29: 199-203.

Bernfield M, Gotte M, Park PW, Reizes O, Fitzgerald ML, Lincecum J, Zako M. 1999. Functions of cell surface heparan sulphate proteoglycans. *Annu. Rev. Biochem.* 68:729-777.

Colliec-Jouault S, Chevolot L, Helley D, Ratiskol J, Bros A, Sinquin C, Roger O and Fischer AM. 2001. Characterization, chemical modifications and in vitro anticoagulant properties of an exopolysaccharide produced by Alteromonas infernus. *Biochim Biophys Acta.* 1528: 141–151.

Downey ME, Holliday LS, Aguirre JI, Wronski TJ. 2009. In vitro and in vivo evidence for stimulation of bone resorption by an EP4 receptor agonist and basic fibroblast growth factor: Implications for their efficacy as bone anabolic agents. *Bone.* 44: 266-274.

Eswarakumar VP, Lax I, Schlessinger J. 2005. Cellular signaling by fibroblast growth factor receptors. *Cytokine GrowthFactor Rev.* 16: 139–149.

Franz, G and Alban S. 1995. Structure-activity relationship of antithrombotic polysaccharide derivatives. *Int. J. Biol. Macromol.* 17: 311-314.

Gallagher JT. 2006. Multiprotein signalling complexes: regional assembly on heparin sulphate. *Biochem. Soc. Trans.* 34: 438-441.

Guezennec JG, Pignet P, Lijour Y, Gentric E, Ratiskol J, Colliec-Jouault S. 1998. Sulphation and depolymerization of a bacterial exopolysaccharide from hydrothermal origin. *Carbohydr Polymers.* 37: 19–24.

Guezennec J. 2002. Deep-sea hydrothermal vents: a new source of innovative bacterial exopolysaccharides of biotechnological interest? *J Ind Microbiol Biotechnol.* 29: 204–208.

Haupt LM, Murali S, Mun FK, Teplyuk N, Mei LF, Stein GS, van Wijnen AJ, Nurcombe V, Cool SM. 2009. The heparan sulphate proteoglycan (HSPG) glypican-3 mediates commitment of MC3T3-E1 cells toward osteogenesis. *J Cell Physiol.* 220: 780-791.

Irie A, Takami M, Kubo H, Sekino-Suzuki N, Kasahara, K, Sanai Y. 2007. Heparin enhances osteoclastic bone resorption by inhibiting osteoprotegerin activity. *Bone.* 41: 165- 174.

Jackson RA, Murali S, van Wijnen AJ, Stein GS, Nurcombe V, Cool SM. 2007. Heparan sulphate regulates the anabolic activity of MC3T3-E1 preosteoblast cells by induction of Runx2. *J Cell Physiol.* 210: 38-50.

Kanzaki S, Takahashi T, Kanno T, Ariyoshi W, Shinmyouzu K, Tujisawa T, Nishihara T. 2008. Heparin inhibits BMP-2 osteogenic bioactivity by binding to both BMP-2 and BMP receptor. *J Cell Physiol.* 216: 844-850.

Karsenty G. 2001. Minireview: transcriptional control of osteoblast differentiation. *Endocrinology.* 142: 2731-2733.

Kong YY, Yoshida H, Sarosi I, Tan HL, Timms E, Capparelli C, Morony S, Oliveira-dos-Santos AJ, Van G, Itie A, *et al.* 1999. OPGL is a key regulator of osteoclastogenesis, lymphocyte development and lymph-node organogenesis. *Nature.* 397: 315-323.

Kram V, Zcharia E, Yacoby-Zeevi O, Metzger S, Chajek-Shaul T, Gabet Y, Müller R, Vlodavsky I, Bab I. 2006. Heparanase is expressed in osteoblastic cells and stimulates bone formation and bone mass. *J Cell Physiol.* 207: 784-792.

Kumarasuriyar A, Lee I, Nurcombe V, Cool SM. 2009. De-sulphation of MG-63 cell glycosaminoglycans delays in vitro osteogenesis, up-regulates cholesterol synthesis and disrupts cell cycle and the actin cytoskeleton. *J Cell Physiol.* 219: 572-583.

Kwan Tat S, Padrines M, Theoleyre S, Heymann D, Fortun Y. 2004. IL-6, RANKL, TNF-alpha/IL-1: interrelations in bone resorption pathophysiology. *Cytokine Growth Factor Rev.* 15: 49–60.

Kwan Tat S, Padrines M, Théoleyre S, Couillaud-Battaglia S, Heymann D, Redini F, Fortun Y. 2006. OPG/membranous--RANKL complex is internalized via the clathrin pathway before a lysosomal and a proteasomal degradation. *Bone*, 39: 706-715.

Lamoureux F, Baud'huin M, Duplomb L, Heymann D, Redini F. 2007. Proteoglycans: key partners in bone cell biology. *Bioessays.* 29 : 758-771.

Lamoureux F, Picarda G, Garrigue-Antar L, Baud'huin M, Trichet V, Vidal A, Miot-Noirault E, Pitard B, Heymann D, Redini F. 2009. Glycosaminoglycans as potential regulators of osteoprotegerin therapeutic activity in osteosarcoma. *Cancer Res.* 69: 526-536.

Ling L, Dombrowski C, Foong KM, Haupt LM, Stein GS, Nurcombe V, van Wijnen AJ, Cool SM. 2010. Synergism between Wnt3a and heparin enhances osteogenesis via a phosphoinositide 3-kinase/Akt/RUNX2 pathway. *J Biol Chem.* [Epub ahead of print]

Manton KJ, Sadasivam M, Cool SM, Nurcombe V. 2006. Bone-specific heparan sulphates induce osteoblast growth arrest and downregulation of retinoblastoma protein. *J Cell Physiol.* 209: 219-229.

Manton KJ, Leong DF, Cool SM, Nurcombe V. 2007. Disruption of heparan and chondroitin sulphate signaling enhances mesenchymal stem cell-derived osteogenic differentiation via bone morphogenetic protein signaling pathways. *Stem Cells.* 25: 2845-2854.

Marie PJ. 2003. Fibroblast growth factor signaling controlling osteoblast differentiation. *Gene*. 316: 23-32.

Matou S, Colliec-Jouault S, Galy-Fauroux I, Ratiskol J, Sinquin C, Guezennec J, Fischer AM, Helley D. 2005. Effect of an oversulphated exopolysaccharide on angiogenesis induced by fibroblast growth factor-2 or vascular endothelial growth factor in vitro. *Biochem Pharmacol*. 69: 751-759.

Mayer AM, Lehmann VK. 2001. Marine pharmacology in 1999: antitumor and cytotoxic compounds. *Anticancer Res*. 21: 2489-2500.

Miraoui H, Oudina K, Petite H, Tanimoto Y, Moriyama K, Marie PJ. 2009. Fibroblast growth factor receptor 2 promotes osteogenic differentiation in mesenchymal cells via ERK1/2 and protein kinase C signaling. *J Biol Chem*. 284: 4897-4904.

Miyazaki T, Miyauchi S, Tawada A, Anada T, Matsuzaka S, Suzuki O. 2008. Oversulphated chondroitin sulphate-E binds to BMP-4 and enhances osteoblast differentiation. *J Cell Physiol*. 217: 769-777.

Mosheimer BA, Kaneider NC, Feistritzer C, Djanani AM, Sturn DH, Patsch JR, Wiedermann CJ. 2005. Syndecan-1 is involved in osteoprotegerin-induced chemotaxis in human peripheral blood monocytes. *J. Clin. Endocrinol. Metab*. 90 : 2964-2971.

Muir JM, Andrew M, Hirsh J, Weitz JI, Young E, Deschamps P, Shaughnessy SG. 1996. Histomorphometric analysis of the effects of standard heparin on trabecular bone in vivo. *Blood*. 88: 1314-1320.

Muir JM, Hirsh J, Weitz JI, Andrew M, Young E, Shaughnessy SG. 1997. A histomorphometric comparison of the effects of heparin and low-molecular-weight heparin on cancellous bone in rats. *Blood*. 89: 3236-3242.

Nakano, K., Okada, Y., Saito, K., Tanaka, Y., 2004. Induction of RANKL expression and osteoclast maturation by the binding of fibroblast growth factor 2 to heparan sulphate proteoglycan on rheumatoid synovial fibroblasts. *Arthritis Rheum*. 50: 2450-2458.

Nichols CA, Guezennec J, Bowman JP. 2005. Bacterial exopolysaccharides from extreme marine environments with special consideration of the southern ocean, sea ice, and deep-sea hydrothermal vents: a review. *Mar Biotechnol (NY)* 7: 253-271.

Raguénès G, Peres A, Ruimy R, Pignet P, R Christen R, Loaec M, Rougeaux H, Barbier G and Guezennec J. 1997. *Alteromonas infernus* sp.nov, a new polysaccharide producing bacterium isolated from a deep-sea hydrothermal vent. *J. Appl. Bacteriol*. 82: 422-430

Rajgopal, R., Bear, M., Butcher, M. K., Shaughnessy, S. G., 2008. The effects of heparin and low molecular weight heparins on bone. *Thromb. Res*. 12:, 293-298.

Roger O, Kervarec N, Ratiskol J, Colliec-Jouault S, Chevolot L. 2004. Structural studies of the main exopolysaccharide produced by the deep-sea bacterium Alteromonas infernus. *Carbohydr Res*. 229: 2371–2380.

Rousselle AV, Heymann D. 2002. Osteoclastic acidification pathways during bone resorption. *Bone*. 30: 533-540.

Ruiz Velasco C., Colliec-Jouault S., Redini F, Heymann D., Padrines M. 2010, Proteoglycans on bone tumor development. *Drug Discov. Today*. 15: 553-560.

Shinmyouzu K, Takahashi T, Ariyoshi W, Ichimiya H, Kanzaki S, Nishihara T. 2007. Dermatan sulphate inhibits osteoclast formation by binding to receptor activator of NF-kappa B
ligand. *Biochem. Biophys. Res. Commun*. 354: 447-452.

Simonet WS, Lacey DL, Dunstan CR, Kelley M, Chang MS, Luthy R, Nguyen HQ, Wooden S, Bennett L, Boone T *et al*. 1997. Osteoprotegerin: a novel secreted protein involved in the regulation of bone density. *Cell.* 89: 309-319.

Standal T, Seidel C, Hjertner O, Plesner T, Sanderson RD, Waage A, Borset M, Sundan A. 2002. Osteoprotegerin is bound, internalized, and degraded by multiple myeloma cells. *Blood.* 100: 3002-3007.

Sutherland IW. 1996. Biotechnology Second, completely revised edition, vol. 6, Products of primary metabolism, Rehm H. J. and Reed G. (eds), VCH, Weinheim, pp. 613-657.

Theoleyre S, Kwan Tat S, Vusio P, Blanchard F, Gallagher J, Ricard-Blum S, Fortun Y, Padrines M, Redini F, Heymann D. 2006. Characterization of osteoprotegerin binding to glycosaminoglycans by surface plasmon resonance: role in the interactions with receptor activator of nuclear factor kappaB ligand (RANKL) and RANK. *Biochem. Biophys. Res. Commun.* 34: 460-467.

Wittrant Y, Théoleyre S, Chipoy C, Padrines M, Blanchard F, Heymann D, Rédini F. 2004. RANKL/RANK/OPG: new therapeutic targets in bone tumours and associated osteolysis. *Biochim Biophys Acta.* 1704: 49-57.

Xiao L, Sobue T, Esliger A, Kronenberg MS, Coffin JD, Doetschman T, Hurley MM., 2010. Disruption of the Fgf2 gene activates the adipogenic and suppresses the osteogenic program in mesenchymal marrow stromal stem cells. *Bone*. 47: 360-370.

Yasuda H, Shima N, Nakagawa N, Mochizuki SI, Yano K, Fujise N, Sato Y, Goto M, Yamaguchi K, Kuriyama M, *et al*. 2004. Identity of osteoclastogenesis inhibitory factor (OCIF) and osteoprotegerin (OPG): a mechanism by which OPG/OCIF inhibits osteoclastogenesis in vitro. *Endocrinology.* 139: 1329-1337.

Zhao B, Katagiri T, Toyoda H, Takada T, Yanai T, Fukuda T, Chung UI, Koike T, Takaoka K, Kamijo R. 2006. Heparin potentiates the in vivo ectopic bone formation induced by bone morphogenetic protein-2. *J Biol Chem*. 281: 23246-23253.

Figure Legends

Figure 1: Branched nonasaccharidic repetitive unit of native EPS.

Figure 2: OS-EPS inhibits BMSCs proliferation during osteoblastic differentiation. BMSCs were incubated in osteogenic media in the presence of 25µg/ml EPS or OS-EPS. After 7 days, images of treated cells were taken under light microscopy (**A**) and the number of viable cells was determined by trypan blue counting (*: p< 0.01) (**B**). Cumulative mitosis of the first 48h of incubation with of EPS or OS-EPS were manually scored from time-lapse analysis (**C**). Cell cycle distribution of BMSCs incubated with EPS or OS-EPS for 48 h was analyzed by propidium iodide staining and FACS analysis (**D**).

Figure 3: OS-EPS inhibits the extracellular matrix mineralization from BMSCs in a dose-dependent manner. (**A**) BMSCs were incubated in osteogenic media for three weeks in the presence or absence of increased concentrations of EPS and OS-EPS. (**B**) EPS or OS-EPS at 25µg/ml were added at different times of the culture period as indicated. At the end of the culture period, Alizarin Red staining was performed (original magnification x 10). (**C**) Gene expression profiles of bone-specific markers of osteoblastic differentiation were determined by qPCR in absence (CT) or in presence of different OS-EPS concentration, The data represent fold difference in expression following normalization against Cyc1.

Figure 4: OS-EPS inhibits RANKL-induced osteoclatogenesis and cell adhesion of human CD14^{+} monocytes. (**A**) CD14^{+} purified monocytes were first cultured for 3 days in 25 ng/ml hM-CSF to achieve a complete cell adhesion. For osteoclastogenesis experiments, cells were then incubated for 15 days in the presence of 25 ng/ml hM-CSF with or without hRANKL (100 ng/ml). EPS or OS-EPS (0,5µg/ml) were added at different time points during

the culture period, as indicated: -3 days indicates the culture condition with only 25 ng/ml of hM-CSF (cellular adhesion period); 0→14 days indicate the period with 25 ng/ml of hM-CSF and 100 ng/ml of RANKL (Osteoclastic differentiation period). At the end of the culture period, TRAP staining was performed (original magnification x 40) and TRAP positives multinucleated cells (more than 3 nuclei) were counted under a light microscope. (**B**) For adherence experiments, cells were incubated for 5 days in the presence of EPS or OS-EPS at 1μg/ml. The non-adherent cells in the supernant were counted in triplicate by using blue trypan exclusion dye. The adherent cells were washed three times in 1x Dulbecco phosphate-buffered saline (DPBS), trypsinised and counted as above.

Figure 5: OS-EPS binds RANKL. Experiments were carried out on a BIAcore 3000 instrument (BIAcore). GAGs (20μM), or EPS (20 μM), or OS-EPS (2μM) were injected at a flow rate of 30 μl/min over the immobilized-RANKL sensorchip (**A**). RANK (2μg/ml), or RANKL (0.5μg/ml) or OS-EPS (200nM) or OPG (1μg/ml) were injected at a flow rate of 30 μl/min over the immobilized-RANKL sensorchip (**B, D**) or over the immobilized-RANK (**C**) or over the immobilized-OPG (**E**). EPS and OS-EPS K_D values for immobilized OPG, RANK and RANKL were assessed (**Table**).

Figure 6: OS-EPS facilitates the binding of RANK-RANKL. Real-time SPR binding analyses of interactions of RANK and RANKL pre-incubated or not with OS-EPS. Sensorgrams were recorded with RANKL (**A**) or RANKL pre-incubated with OS-EPS (**B**) immobilized on CM5 sensor chips, and injections of RANK solutions [50, 25, 12.5, 6.25, and 3.125 nM RANK], using a BIAcore 3000 biosensor and BiaEval 4.1 software. The kinetic and thermodynamic values were ka $(M^{-1}s^{-1})$ = 5.28 10^5; kd (s^{-1}) = 1.27 10^{-3} and K_D = 2.39 nM for

RANKL in (**A**), and ka $(M^{-1}s^{-1}) = 1.23\ 10^6$; kd $(s^{-1}) = 1.32\ 10^{-3}$ and $K_D = 1.09$ nM for RANKL pre-incubated with OS-EPS in (**B**).

Figure 7: OS-EPS reduces trabecular bone. Twenty four 4-week-old male C3H/HeN male mice received daily s.c. injection of DPBS, EPS, OS-EPS or heparin (6 mg/kg) for a period of 28 days. (**A**) Right femur of each animal was dissected for microarchitectural parameter quantification. The distal metaphysis were used for micro-computed tomography (μ-CT) on a SkyScan-1072 (SkyScan, Aartselaar, Belgium). μCT-Analyser software SkyScan was used to analyse the structure of the samples. Bone volume ratio (BV/TV), trabecular thickness (Tb.Th), trabecular number (Tb.N) and trabecular separation (Tb.Sp) were assessed (**Table**). (n= 6 by groups). (*: $p < 0.05$). (**B**) Analysis and quantification of osteoblastic and osteoclastic areas were done using a Leica Q500 image analysis system after TRAP and ALP staining, respectively. Two independent experiments were performed (n= 6 by groups). (*: $p < 0.05$).